



Report No. 5005.0486A

May 14, 2015

**METALLURGICAL EVALUATION OF TANK COUPON T396-F/S9/10 FROM  
FREEDOM INDUSTRIES, CHARLESTOWN, WEST VIRGINIA**

Customer Authorization: CSB2014-01-I-WV

Report To: U.S. Chemical Safety and Hazard Investigation Board

Attn: [REDACTED]

2175 K Street, NW, Suite 400

Washington, D.C. 20037

---

## **1.0 INTRODUCTION**

One section of chemical storage tank bottom and shell, identified as EV-CSB2014-01-I-WV-T396-F/S9/10 from Tank 396, Freedom Industries, Charleston, West Virginia, was submitted by the United States Chemical Safety and Hazard Investigation Board (CSB) for witnessed inspection and laboratory testing. It was reported that Tank 396 was the source of a chemical release into the Elk River, Charleston, West Virginia, on January 9, 2014, and that holes in the tank bottom of the subject section, referred to here as T396-F/S9/10, provided a leak path that enabled the chemical release. Sample T396-F/S9/10 was received at Anamet on May 12, 2014, and the package was not opened until the interested parties were present on September 30, 2014. The inspection and testing was guided by a written protocol developed by the CSB, and took place from September 30 through October 3, 2014 at Anamet, Inc., in Hayward California. Witnesses present on the first day of testing are listed in Table 1.

The subject was evaluated by the following laboratory procedures:

- 1) Visual and macroscopic examination
- 2) Metallography
- 3) Scanning electron microscopy and energy dispersive X-ray spectroscopy
- 4) Chemical analysis
- 5) Tensile testing

Based on the results of this evaluation, holes in the floor of Tank 396 were caused by pitting corrosion that initiated on the inside surface and propagated toward the soil side. Remnants of a poly vinyl acetate coating were present on the inside surface of the tank floor. Chemical analysis indicated the floor met the chemical composition requirements of a range of carbon steels commonly used for welded steel storage tanks. Tensile testing indicated the tank floor met the tensile requirements of a range of carbon steels commonly used for welded steel storage tanks.

**This report shall not be reproduced, except in full, without the written approval of Anamet.**



## 2.0 EVALUATION<sup>1</sup>

### 2.1 Visual Examination

Sample T396-F/S9/10 consisted of a section of nominally 0.25-inch thick tank bottom and joined shell from the location indicated in schematic diagrams shown in Figure 1 and Figure 2. The sample is shown after unpacking in Figure 3 and Figure 4. During the witnessed work, the tank bottom was commonly referred to as the floor. Because the term “floor” was used to identify several specimens taken from the sample, “floor” will be use in place of “bottom” in the remainder of this report.

A light tan colored soil coated both the inside and outside surfaces of the sample as-received. It was reported that during water jet cutting of the tank, the local soil was unavoidably spread onto the sample. A photograph of the shell to floor joint is shown in Figure 5. The joint was completed with fillet welds along the top and outer edge of a steel angle as shown. A small section of welded lap joint between floor plates was present, but in this sample the majority of the floor was from a single plate, and all of the shell was from a single plate.

Holes in the floor are shown in Figure 6. On the inside surface, broad pits were visible next to the holes. Specimens of corrosion product and soil were extracted from the two larger pits onto carbon tape. A dark area was present on the floor soil side adjacent to the holes. The appearance of the dark area suggested the soil was saturated by a substance other than water.

The sample was cleaned with tap water sprayed from a household pressure washer rated at 1900-psi. Care was taken to remove soil and loose rust, but retain corrosion product, particularly within pits. The sample is shown after washing in Figure 7 through Figure 10. Cleaning revealed shallow pits on the floor inside surface that had been obscured by dried soil, examples are indicated in Figure 9a. Three pits were located along an arc extending from the largest hole to the shallowest pit. The cause of this spatial relationship was not apparent based on the available evidence, although the arc was roughly aligned with the plate rolling direction, described in Section 2.6. Therefore, it is possible that the pits initiated along inclusion stringers at or near the steel surface. Based on the contour of the hole edges, the holes initiated on the inside surface as corrosion pits and grew toward the soil side. In general, the corrosion morphology was different on the inside and soil side surfaces. Inside surface morphology was characterized by fields of small pits that created a surface roughness similar to that found within the broad pits adjacent to and within the holes in the floor. Small areas of mill scale were present toward the sample side away from the shell. The soil side morphology was characteristic of general corrosion of carbon steel, with shallow pits and patches of mill scale away from the shell wall.

Remnants of a flexible organic coating were present on the floor inside surface, as shown in Figure 10a. Water was beading on the soil side dark area adjacent to the floor holes, and the surface of this area had a greasy, sticky feel. Specimens of the sticky surface and the organic coating were collected for chemical analysis. Analysis by infrared spectroscopy, described in Section 2.5, determined the inside surface coating to be a vinyl acetate and several possible matches were found for the sticky soil side specimen.

---

<sup>1</sup> The magnifications of the optical and scanning electron micrographs in this report are approximate and should not be used as a basis for dimensional analyses unless otherwise indicated.



Laser scanning was performed on the washed sample to capture a point-cloud model of the floor geometry and surface features prior to sectioning. The laser scanning subcontractor was prepared to scan samples 10-inches by 10-inches in size, as described in the protocol, on a rotating stage. However, upon request, the subcontractor agreed to scan the entire floor section, with the understanding that digital stitching would be required to represent the entire floor portion of the sample because it was too large to fit on the rotating stage. A view of the three dimensional model of the floor inside surface is shown in Figure 11. Although some stitching artifacts were introduced, the general geometry and local detail around the holes and pits was captured.

Thickness measurements were performed on the sample floor section using a pointed anvil micrometer after the floor had been sectioned. Measured thickness and general locations are indicated in Figure 12.

## 2.2 Metallography

Specimens were prepared for metallography from the floor sections indicated in Figure 13. The specimen labeled floor pit is shown as-polished in Figure 14. This sample illustrated the general differences between inside surface and soil side surface corrosion morphology. Within the broad pits on the inside surface, corrosion advanced in cells of localized attack, as shown in Figure 14 and Figure 15.

A specimen labeled floor 1, shown in Figure 16, was prepared from a section through an area of remnant inside surface coating. In cross section, the outer layers of the coating were an opaque light tan color and an inner layer was a translucent amber color, shown in Figure 17a. Significant erosion of the outer layer during polishing indicated water solubility, consistent with the flexibility of specimens pulled from the surface immediately after washing and subsequent stiffness of the specimens after drying. Corrosion product was present beneath the coating, shown in Figure 17b. Examples of mill scale on the floor 1 specimen soil side surface are shown in Figure 18 and Figure 19. In some regions, mill scale was closely adhered to the soil side, and in others, under scale corrosion had separated the scale from the steel surface.

A specimen labeled floor 2, shown in Figure 20a, was prepared through a section through mill scale on the soil side surface. As shown in Figure 20b, some regions of tightly adhered mill scale were present. Examples of inside surface corrosion similar to other areas of the floor are shown in Figure 21.

The general microstructure of the floor, shown in Figure 22, was consistent with low and medium carbon hot finished steels.

## 2.3 Scanning Electron Microscopy and Energy Dispersive X-ray Spectroscopy

Specimens of the floor were examined using a scanning electron microscope (SEM) and analyzed by energy dispersive X-ray spectroscopy<sup>2</sup> (EDS). Spectra from the pit locations

---

<sup>2</sup> The EDS analysis method used here detects the presence of elements from boron (B) to uranium (U), atomic numbers from 5 to 92 in the periodic table. EDS data alone are, however, insufficient to differentiate chemical compounds such as oxides, hydroxides, or carbonates or to characterize organic materials that consist of carbon (C), hydrogen (H), and nitrogen (N) only.



indicated in Figure 13b are shown in Figure 23. Silicon (Si), aluminum (Al), calcium (Ca), titanium (Ti), sulfur (S) potassium (K) and chlorine (Cl) were detected in the corrosion product. The floor pit cross section was analyzed as-cut with a dry band saw, and representative EDS maps and spectra are shown in Figure 24 and Figure 25. Zinc (Zn) was detected within pit corrosion product and mapping showed a correlation between the zinc and sulfur. Mapping indicated chlorine was equally distributed in the corrosion product and on the steel surface. Similar results were obtained from the as-polished surface of the floor pit specimen, as shown in Figure 26 and Figure 27.

Analysis results of the soil side corrosion product of specimen floor 1 are shown in Figure 28 and Figure 29. Sulfur and low levels of zinc were evenly distributed in the mapped area.

## **2.4 X-Ray Diffraction**

After water washing and drying the subject, specimens of corrosion product were scraped from the floor inside and soil side surface locations indicated in Figure 7 and Figure 8. Analysis of the specimens by X-ray diffraction (XRD) was subcontracted to EAG/Evans Analytical. The results are summarized in Table 2 and Table 3, and the complete EAG report is shown in the Appendix. Forms of iron oxide and iron hydroxides consistent with aqueous corrosion of carbon steel were detected in addition to silicates and calcium carbonates that likely originated from the local soil.

## **2.5 Chemical Analysis**

Chemical analysis of the sample floor was performed by optical emission spectroscopy, with carbon and sulfur concentrations determined by combustion analysis. The results, listed in Table 4, were consistent with a number of carbon steels commonly used in welded storage tanks. No particular material specification was reported.

Specimens of the inside surface coating were analyzed by infrared spectroscopy (FTIR). Macrographs of inside surface coating specimen cross sections are shown in Figure 30. Analysis was performed on translucent amber spectrum are shown in Figure 31. The inside surface coating was identified as a vinyl acetate. Similar spectra and spectra library matches, Figure 32, were obtained from a sample identified as EV-CSB2014-01-1-WV-T396 LATEX, FROM BOTTOM OF T396, which consisted of several pounds of material collected from the floor of Tank 396 during initial stages of the investigation at the Freedom Industries site.

A specimen of the floor soil side sticky area adjacent to the holes was analyzed by FTIR. An absorption spectrum and spectra library matches are shown in Figure 33. The best fit library match was to glycerol monooleate and the second best match was to Bis-(2-hydroxyethyl dimerate). There is no obvious correlation between the sticky substance on the floor soil side and inside surface corrosion pits that lead to release of the tank contents.

## **2.6 Tensile Testing**

A tensile test was performed on a specimen from the sample floor. Metallography had been performed on a specimen from the floor to determine the rolling direction, and the tensile specimen was machined with the gage length parallel to the indicated rolling direction, as shown

---



in Figure 13a. Test results, listed in Table 5, were consistent with carbon steels commonly used for welded storage tanks. No particular material specification was reported.

### 3.0 CONCLUSIONS<sup>3</sup>

The following conclusions are based upon the submitted sample and the evidence gathered:

1. Holes in the floor of Tank 396 were caused by pitting corrosion that initiated on the inside surface and propagated toward the soil side.
2. Remnants of a vinyl acetate coating were present on the inside surface of the floor of Tank 396.
3. The floor of Tank 396 met the chemical composition requirements of a range of carbon steels commonly used for welded steel storage tanks.
4. The floor of Tank 396 met the tensile requirements of a range of carbon steels commonly used for welded steel storage tanks.

Prepared by:

Sam McFadden, Ph.D.  
Associate Director of Laboratories

Reviewed by:

Audrey Fasching, Ph.D., P.E.  
Senior Materials Engineer

<sup>3</sup> The conclusions in this report are based upon the available information and evidence provided by the client and gathered by Anamet, within the scope of work authorized by the client, and they are hereby presented by Anamet to a reasonable degree of engineering and scientific certainty. Anamet reserves the right to amend or supplement its conclusions or opinions presented in this report should additional data or information become available, or further work be approved by the client.



Table 1  
Attendance List Derived from Sign In Sheet Dated September 30, 2014

[REDACTED]	[REDACTED]

Table 2  
Summary of XRD Results of Scrapings from the Floor Inside Surface

Floor Inside Surface Sample 1		Floor Inside Surface Sample 2	
Primary Phases	Minor or Trace Phases	Primary Phases	Minor or Trace Phases
Fe <sub>2</sub> O <sub>3</sub>	$\alpha$ -Fe <sup>+3</sup> O(OH) $\gamma$ - Fe <sup>+3</sup> O(OH) Mg <sub>3</sub> Fe <sub>2</sub> (SiO <sub>4</sub> ) <sub>3</sub> SiO <sub>2</sub> CaCO <sub>3</sub>	Mg <sub>3</sub> Fe <sub>2</sub> (SiO <sub>4</sub> ) <sub>3</sub> SiO <sub>2</sub>	Fe <sub>2</sub> O <sub>3</sub> $\alpha$ -Fe <sup>+3</sup> O(OH) $\gamma$ - Fe <sup>+3</sup> O(OH) CaCO <sub>3</sub>

Table 3  
Summary of XRD Results of Scrapings from the Floor Soil Side Surface

Floor Soil Side Surface Sample 1		Floor Soil Side Surface Sample 2	
Primary Phases	Minor or Trace Phases	Primary Phases	Minor or Trace Phases
$\alpha$ -Fe <sup>+3</sup> O(OH) Fe(CO) <sub>3</sub>	CaCO <sub>3</sub> Fe <sub>2</sub> O <sub>3</sub> Fe <sub>9.5</sub> O <sub>14</sub> (OH) <sub>2</sub> SiO <sub>2</sub>	$\alpha$ -Fe <sup>+3</sup> O(OH) Fe(CO) <sub>3</sub>	CaCO <sub>3</sub> Fe <sub>3</sub> O <sub>4</sub> Fe <sub>9.5</sub> O <sub>14</sub> (OH) <sub>2</sub> SiO <sub>2</sub>



Table 4  
Results of Quantitative Chemical Analysis of  
T396-F/S9/10 Floor Specimen

Element	Floor (wt%)
Aluminum (Al)	0.01
Carbon* (C)	0.25
Chromium (Cr)	0.03
Columbium (Cb)	<0.005
Copper (Cu)	0.02
Iron (Fe)	Major Constituent
Manganese (Mn)	0.41
Molybdenum (Mo)	<0.005
Nickel (Ni)	0.01
Phosphorus (P)	0.007
Silicon (Si)	0.04
Sulfur* (S)	0.025
Titanium (Ti)	<0.005
Vanadium (V)	<0.005

\*Carbon and sulfur concentrations determined by combustion analysis, all others determined by optical emission spectroscopy

Table 5  
Tensile Test Results, Tank Floor, Flat Specimen  
0.50-inch Nominal Gage Width, 2.0-inch Nominal Gage Length

Tensile Strength (psi)	63500
Yield Point (psi)	42400
Elongation in 2-inch Gage (%)	28

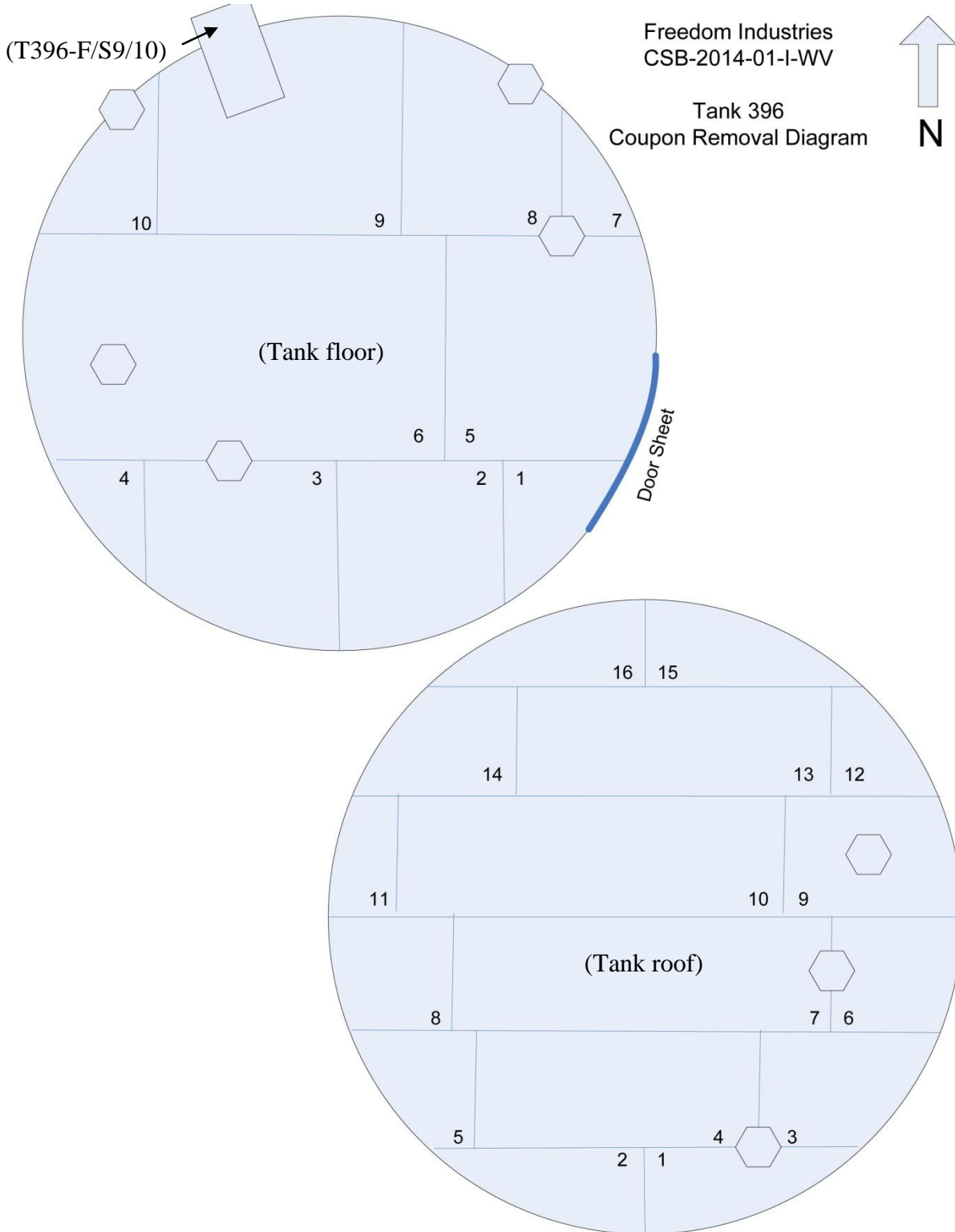


Figure 1 Schematic diagram of Tank 396 bottom and roof. Courtesy of the CSB, notations in parentheses added by Anamet.

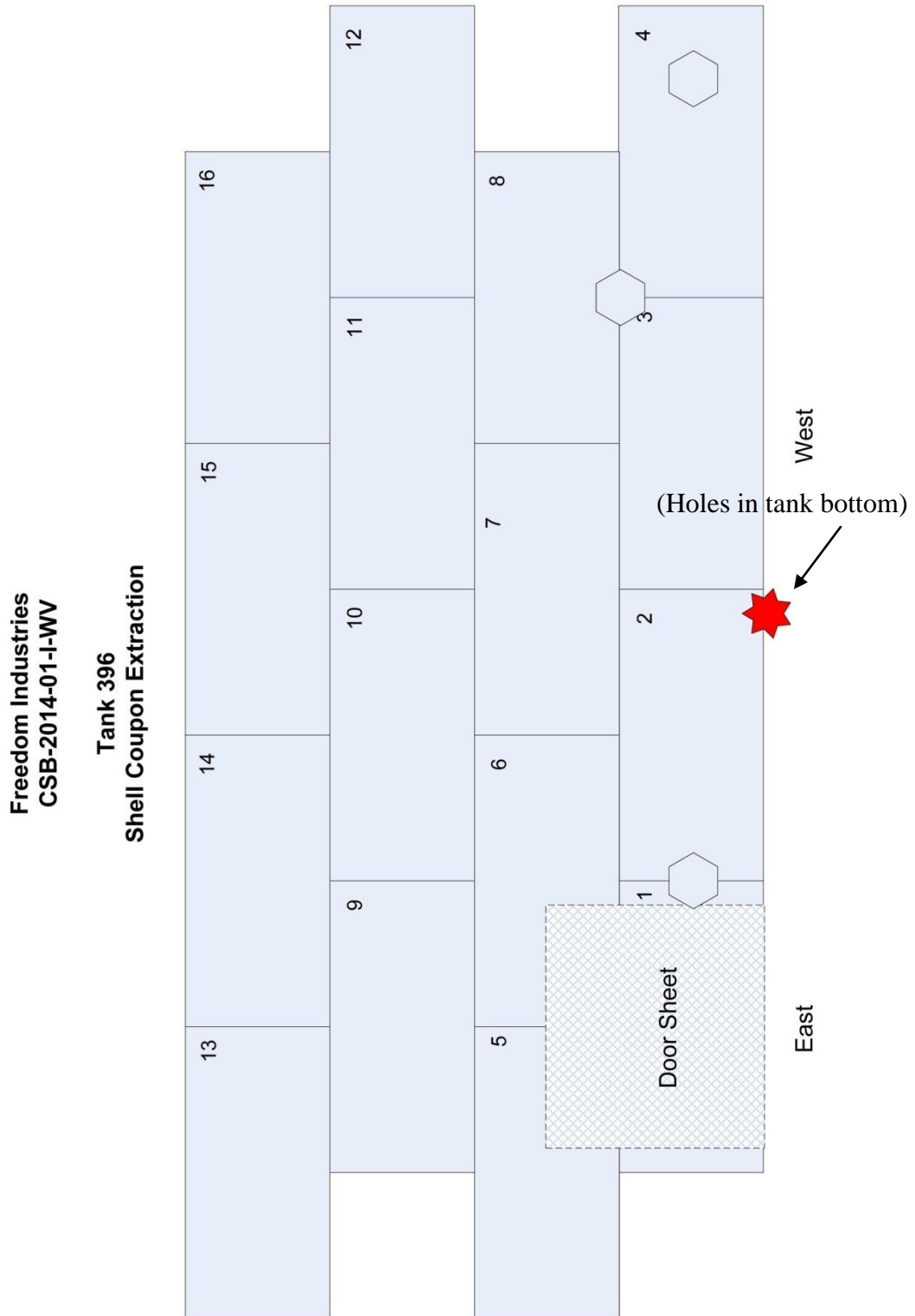


Figure 2 Schematic diagram of Tank 396 shell. Courtesy of the CSB, notation in parentheses added by Anamet.

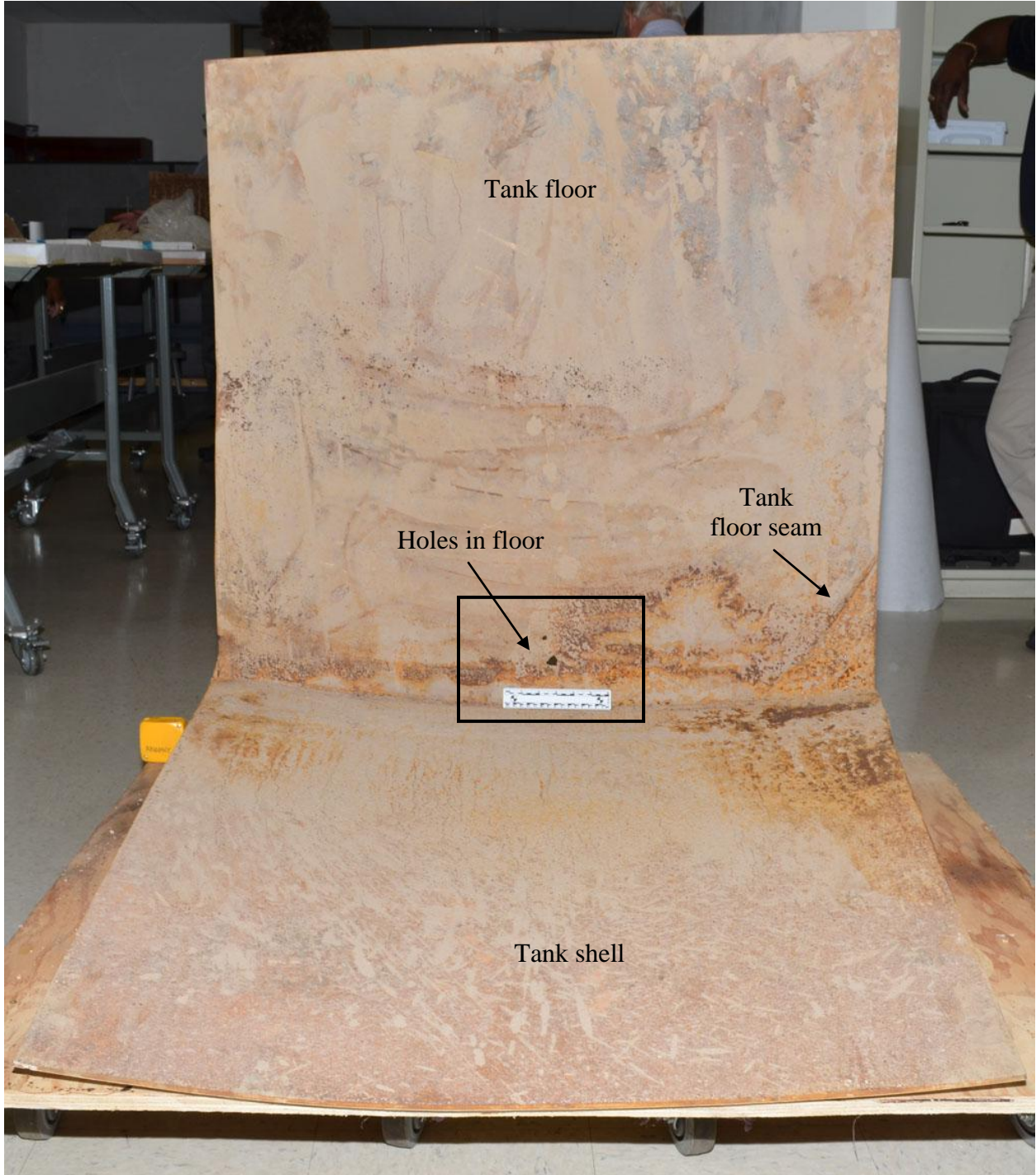


Figure 3 Photograph of the tank inside surface of the sample in the as-received condition after unpacking.

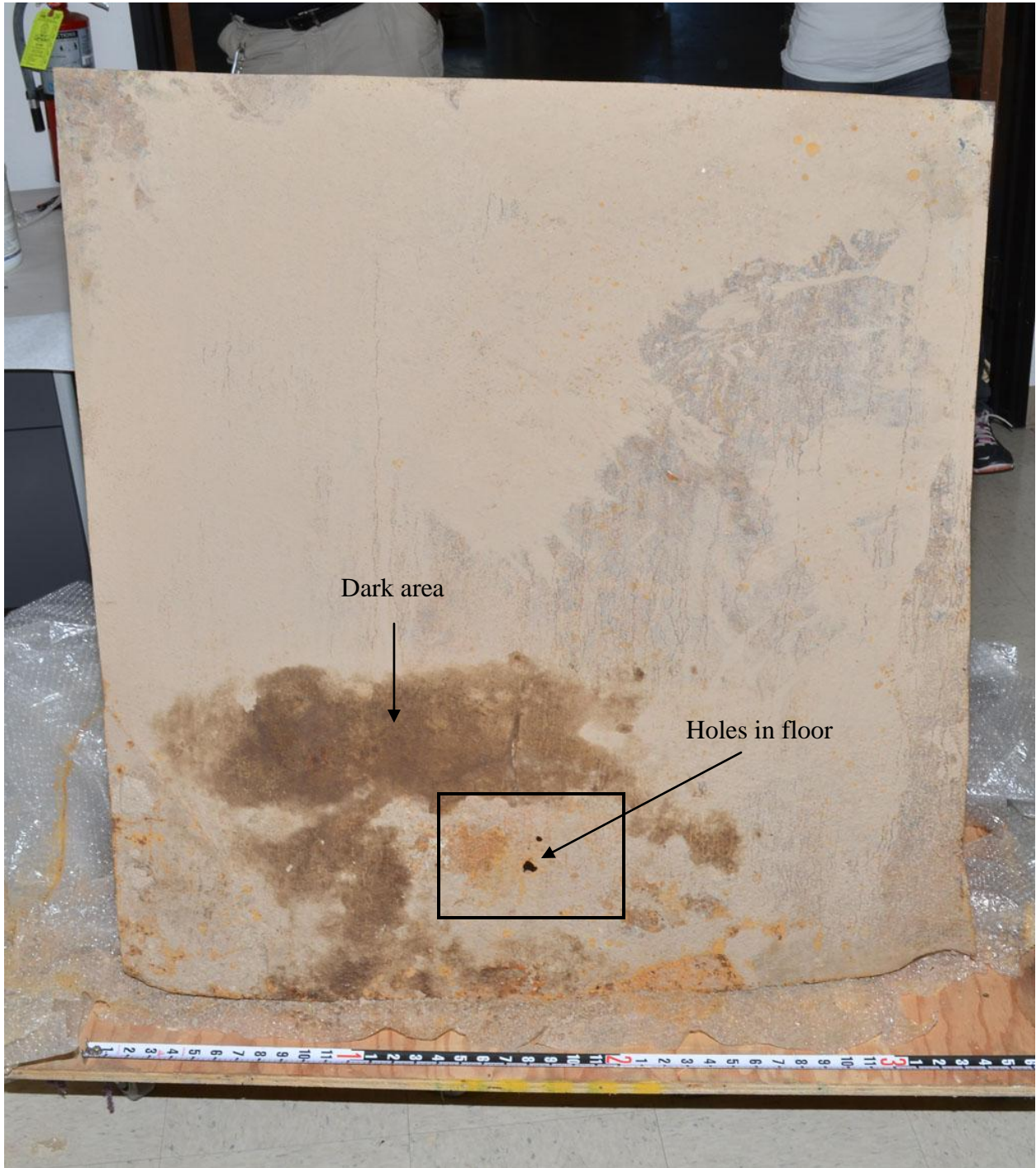
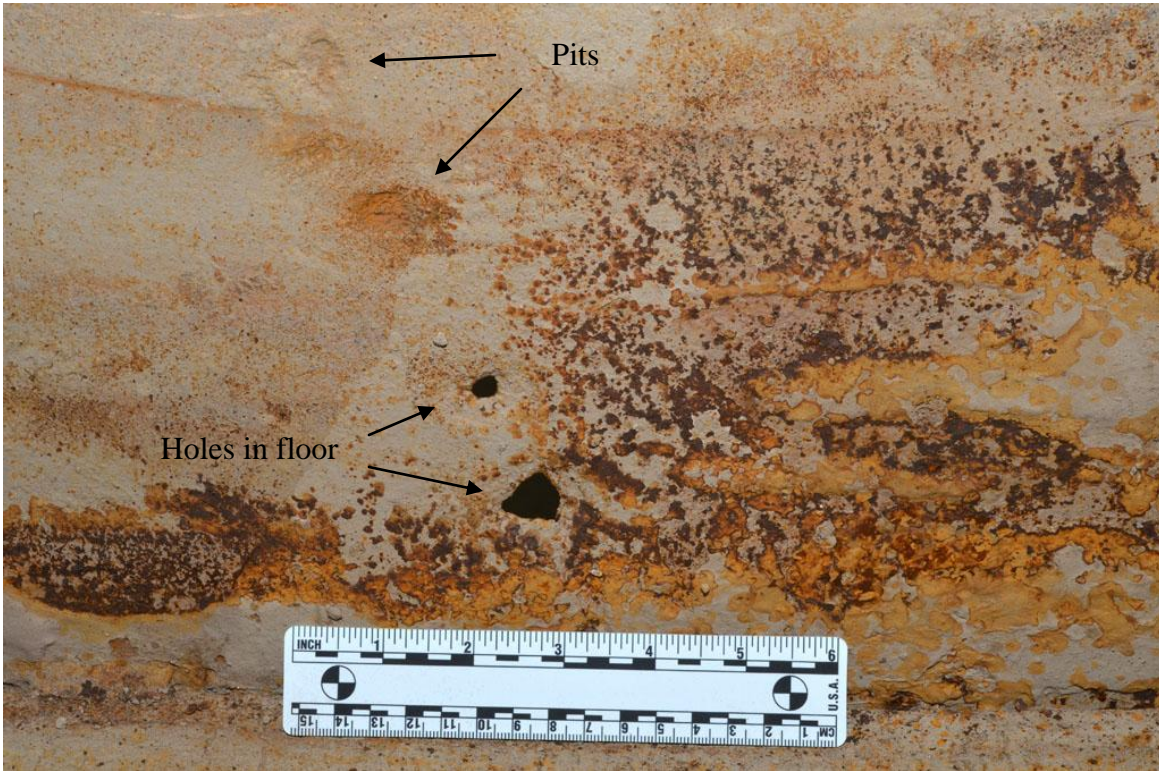


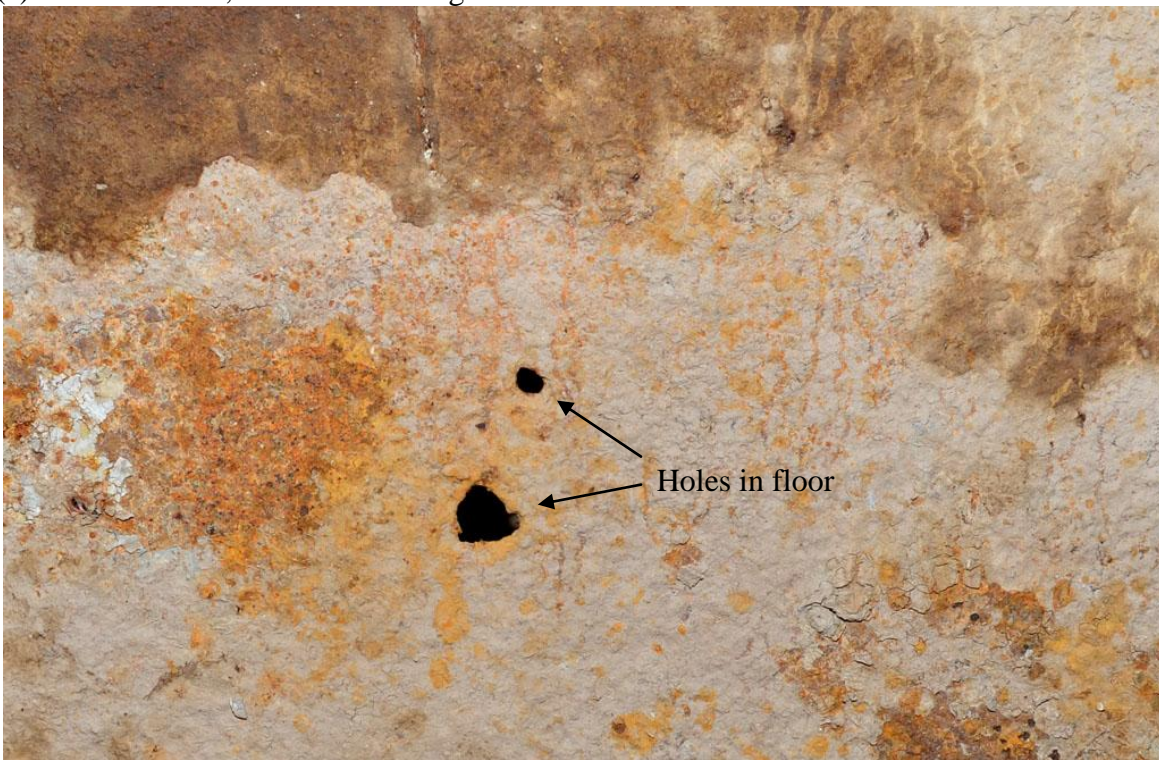
Figure 4 Photograph of floor soil side surface.



Figure 5 Photograph of the floor to wall welded joint.



(a) Inside surface, boxed area in Figure 3



(b) Soil side surface, boxed area in Figure 4

Figure 6 Photographs of the boxed areas in Figure 3 and Figure 4.

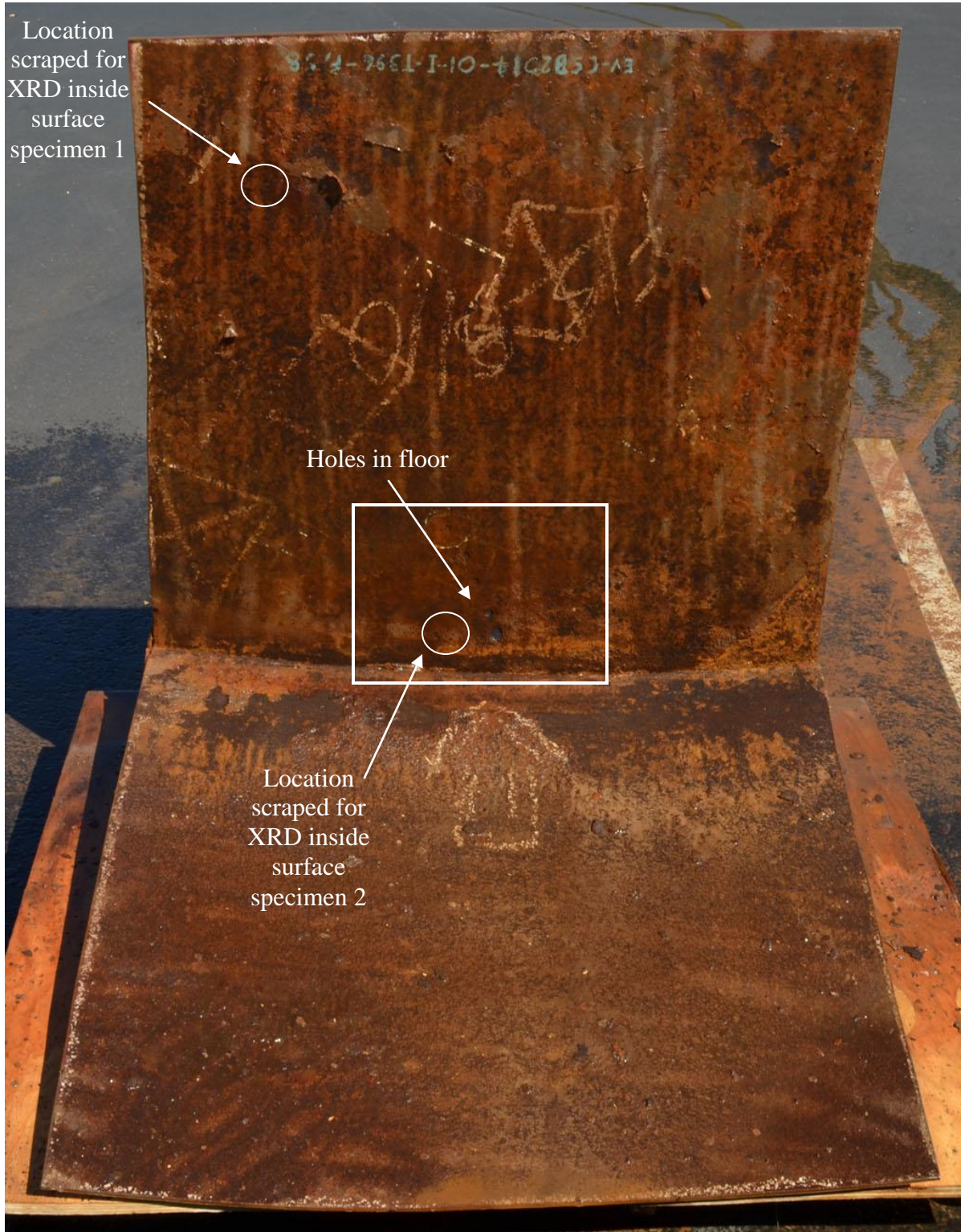


Figure 7 Photograph of the inside surface of the sample after cleaning. Notations written directly on the surface were made at the Freedom Industries incident site.

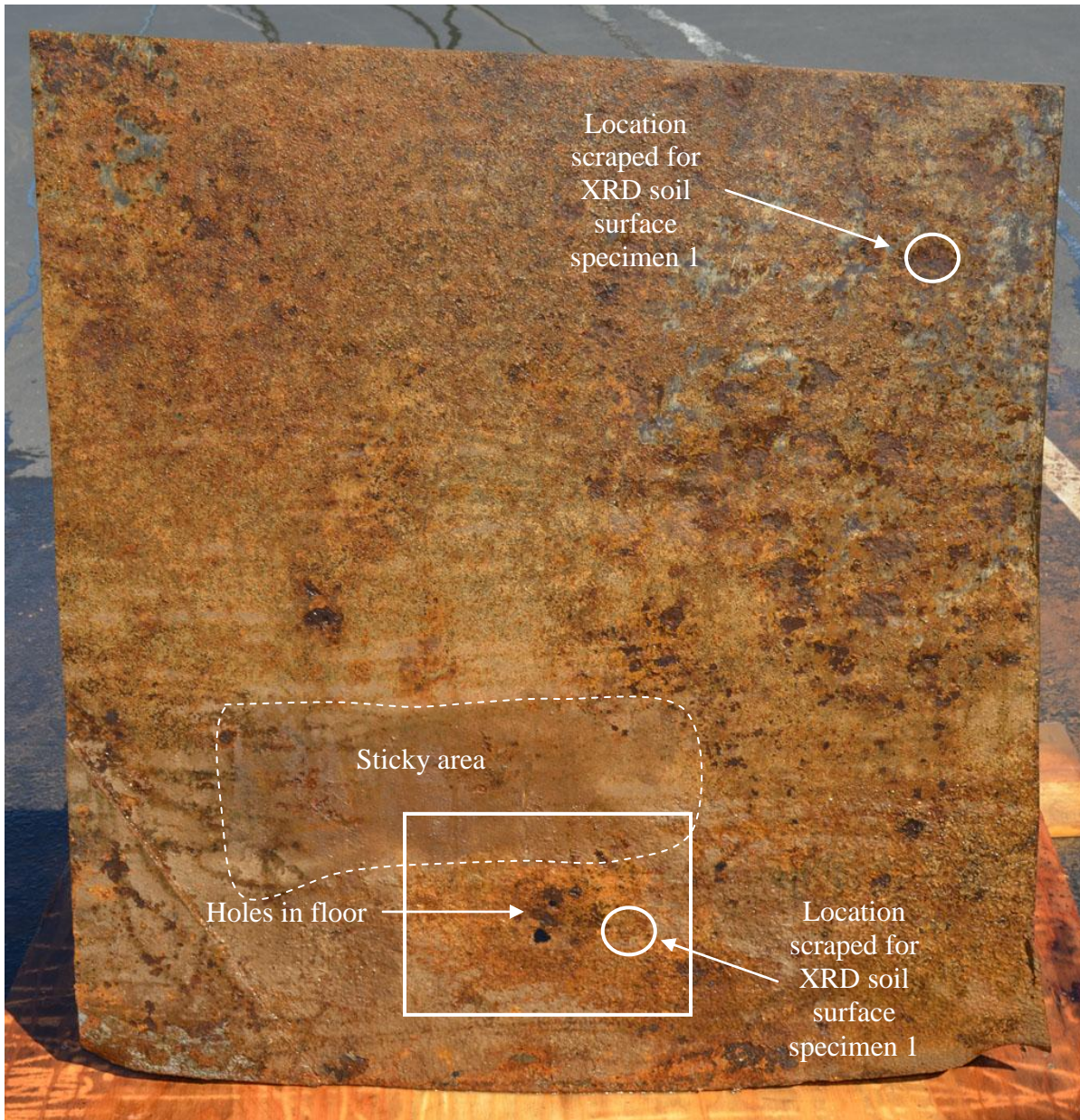
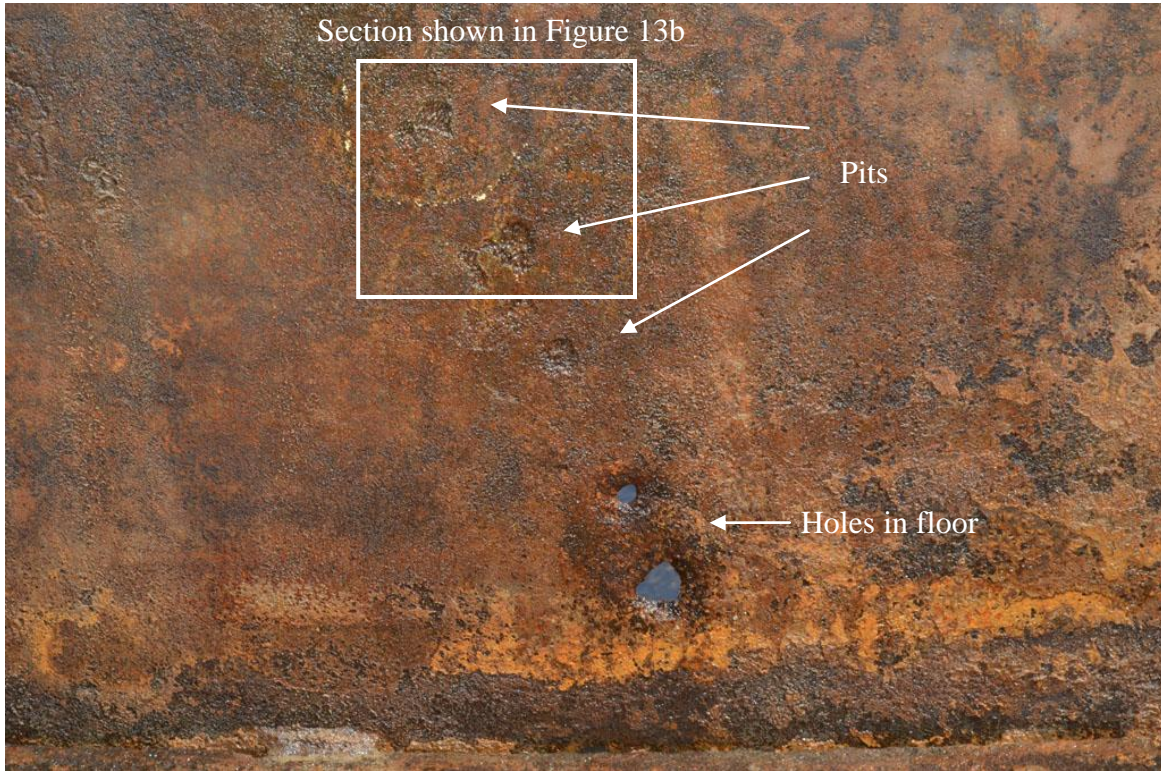
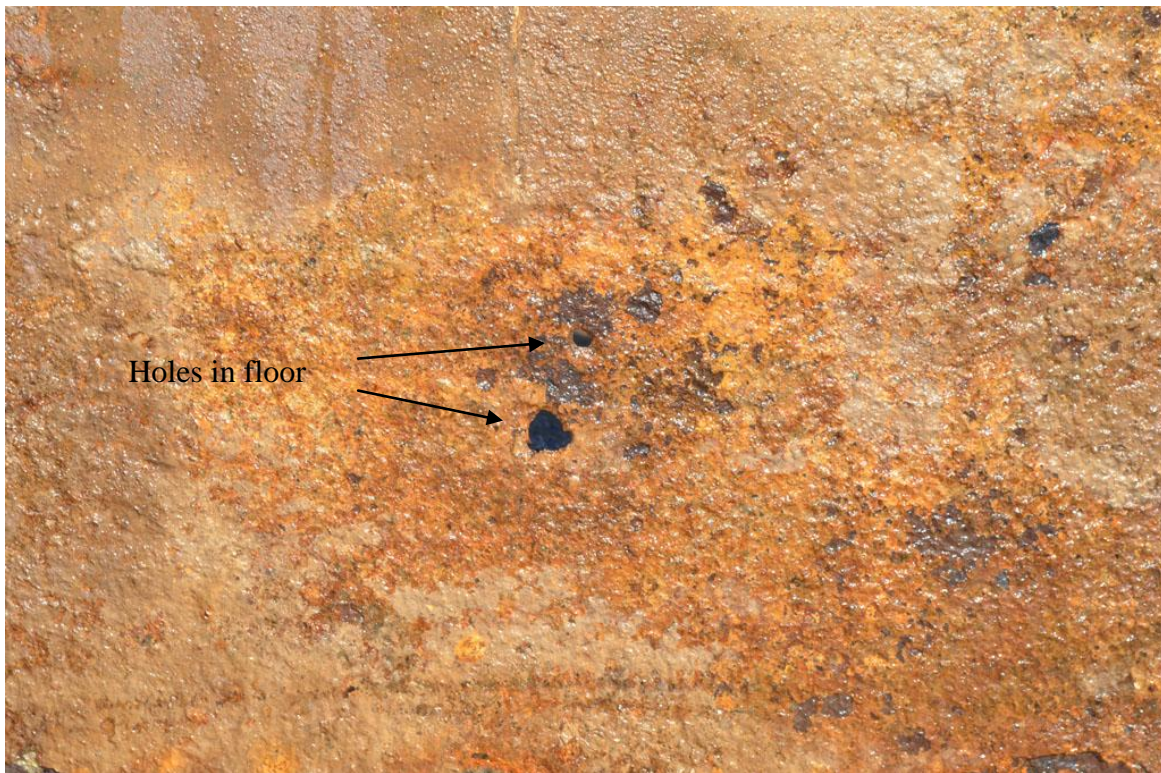


Figure 8 Photograph of the soil side surface of the sample after cleaning.



(a) Inside surface, boxed area in Figure 7



(b) Soil side surface, boxed area in Figure 8

Figure 9      Photographs of the boxed areas in Figure 7 and Figure 8.



(a) Floor inside surface



(b) Floor soil side surface, sticky area

Figure 10 Photographs of (a) coating remnants on the floor inside surface and (b) sticky deposits on the floor soil side surface.

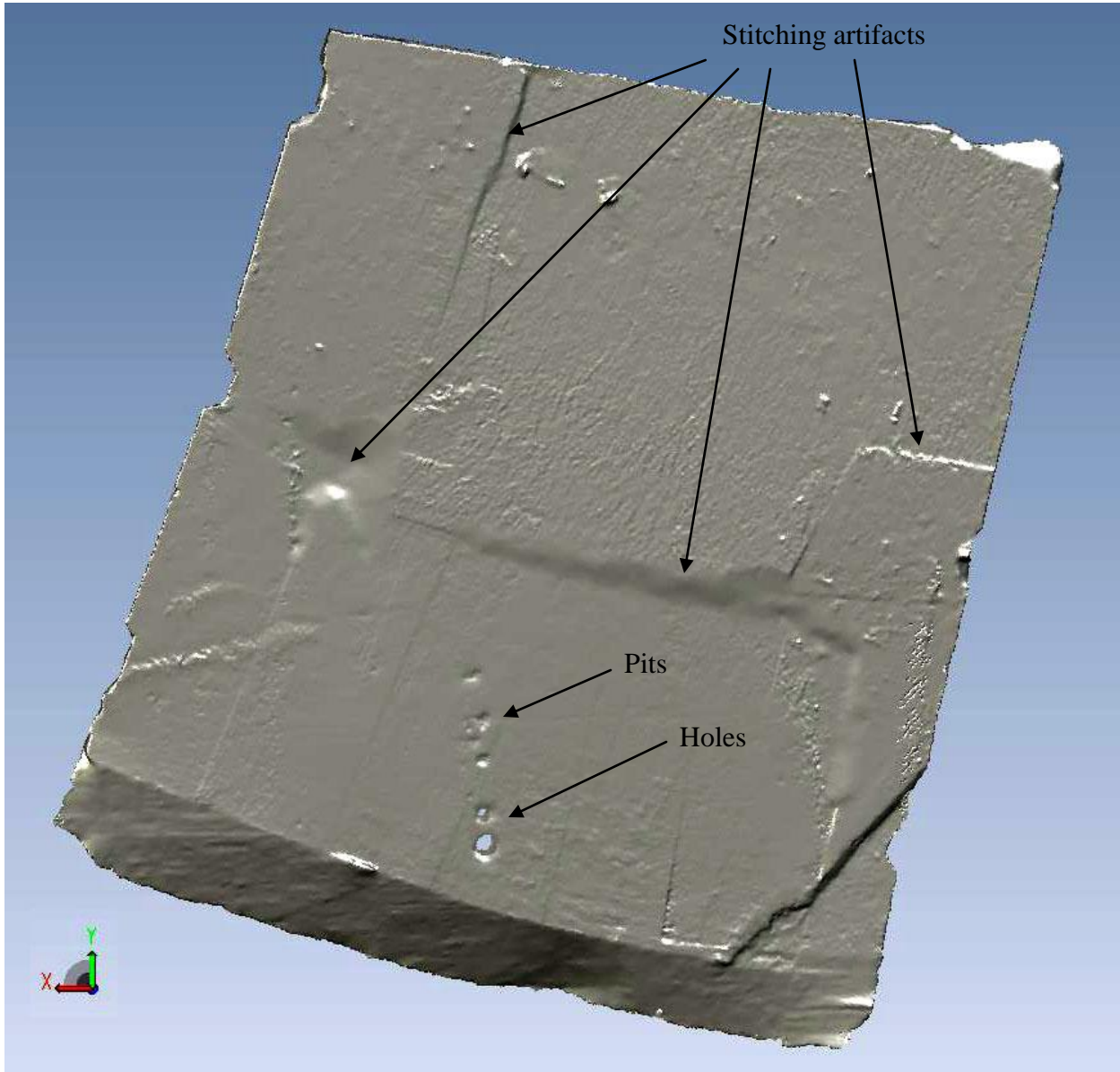


Figure 11 Three dimensional model of the inside surface of the floor obtained from laser scanning.



(a)



(b) Boxed area in (a)

Figure 12 Photographs of the floor with thickness measurements annotated. The measurements were made after the sample had been sectioned as shown in Figure 13a.

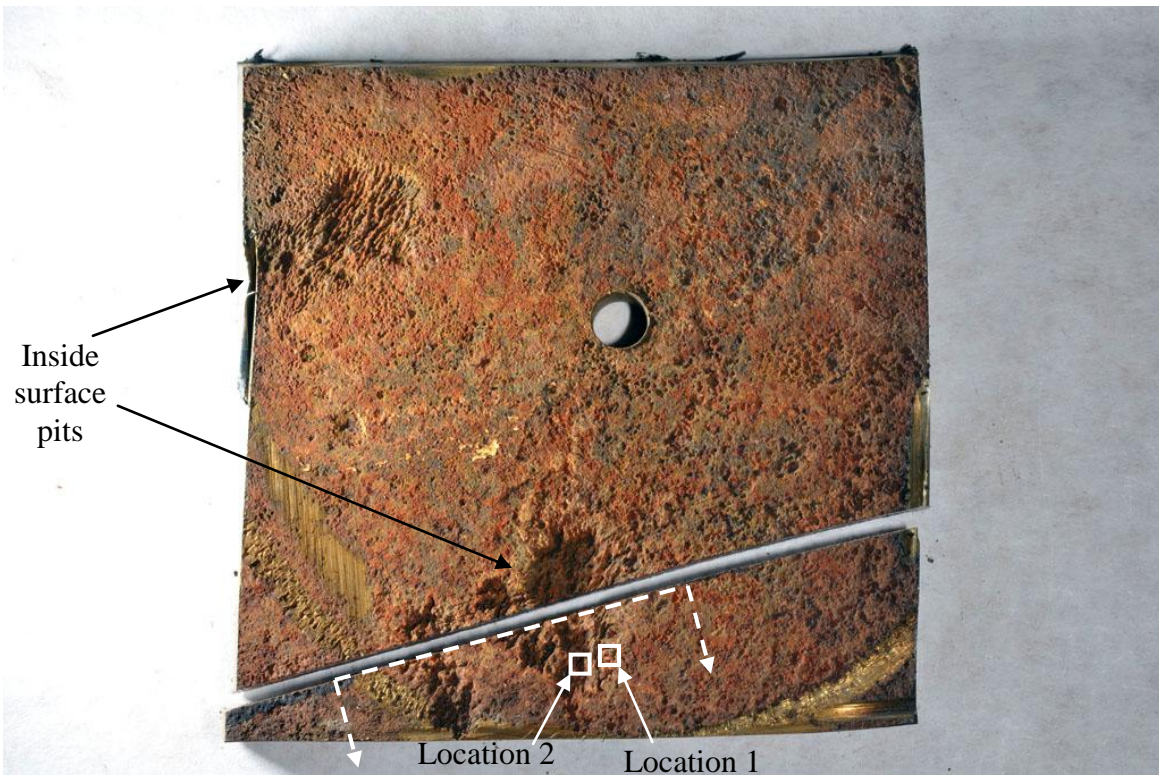
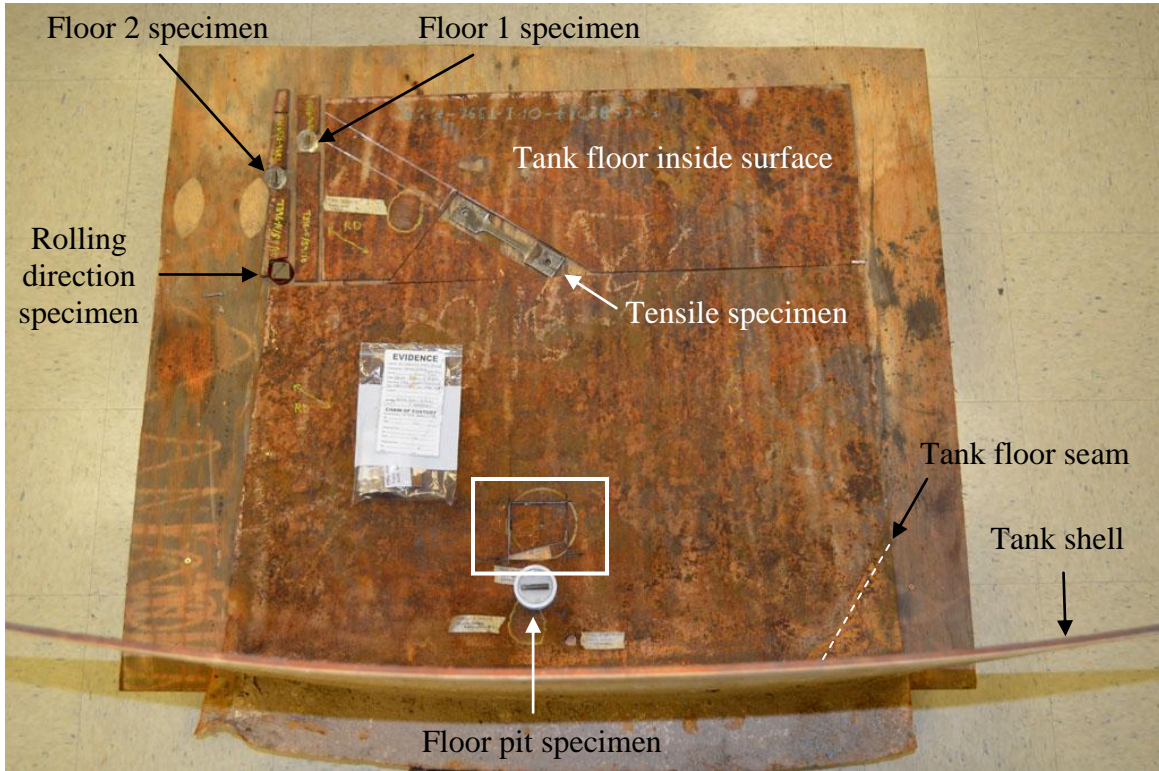
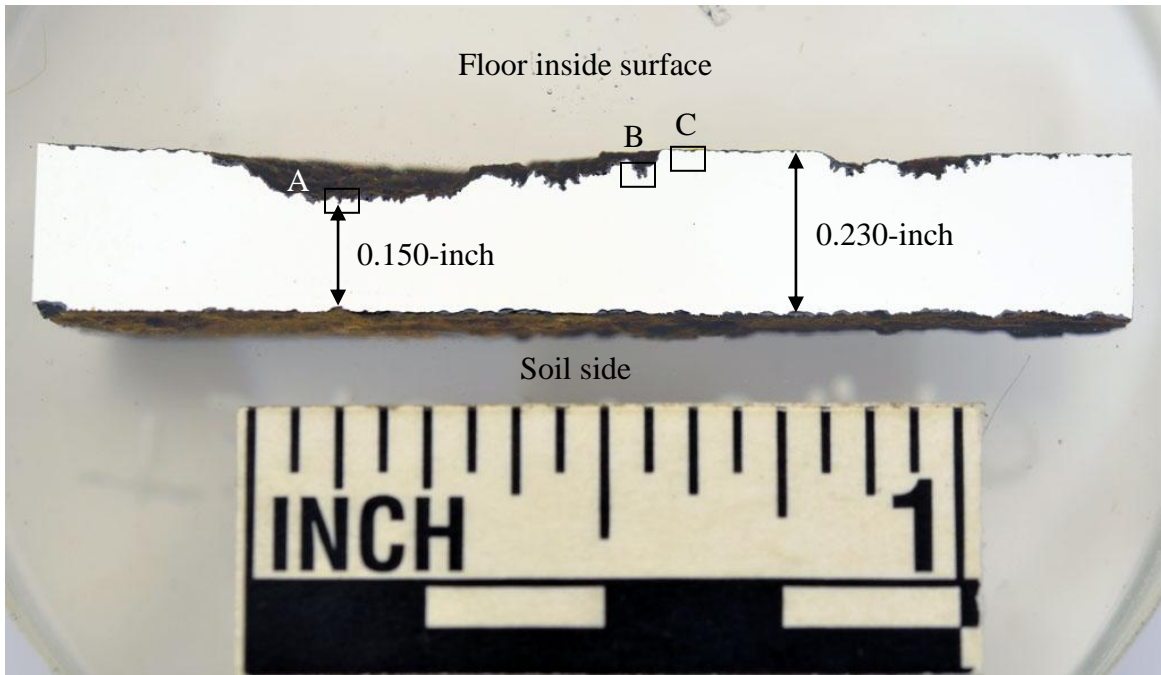
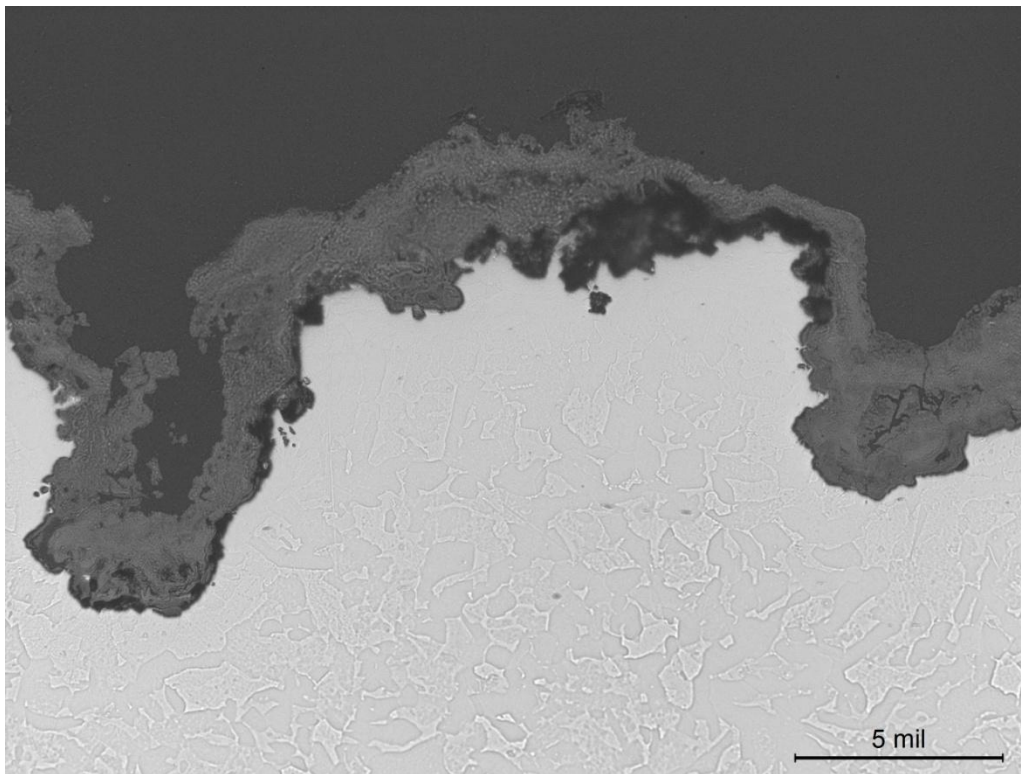


Figure 13 Photographs of sections and specimen locations on the floor of the coupon. The dashed lines in (b) indicate the floor pit section that was prepared for metallography.



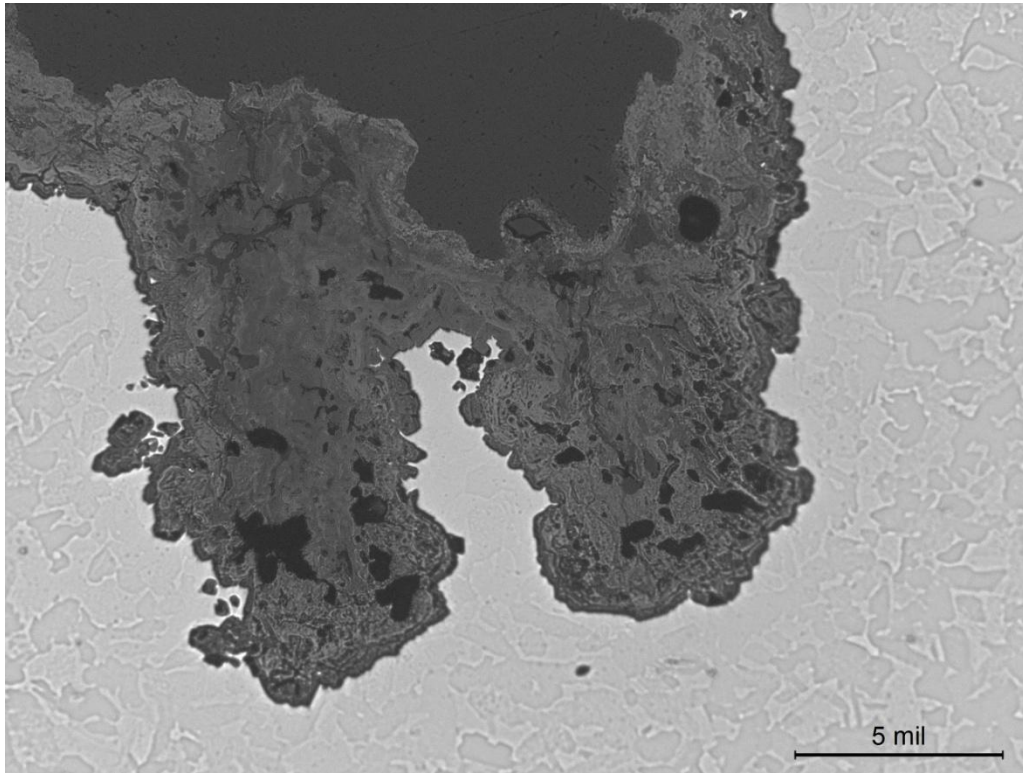
(a) Specimen floor pit



(b) Boxed area A in (a)

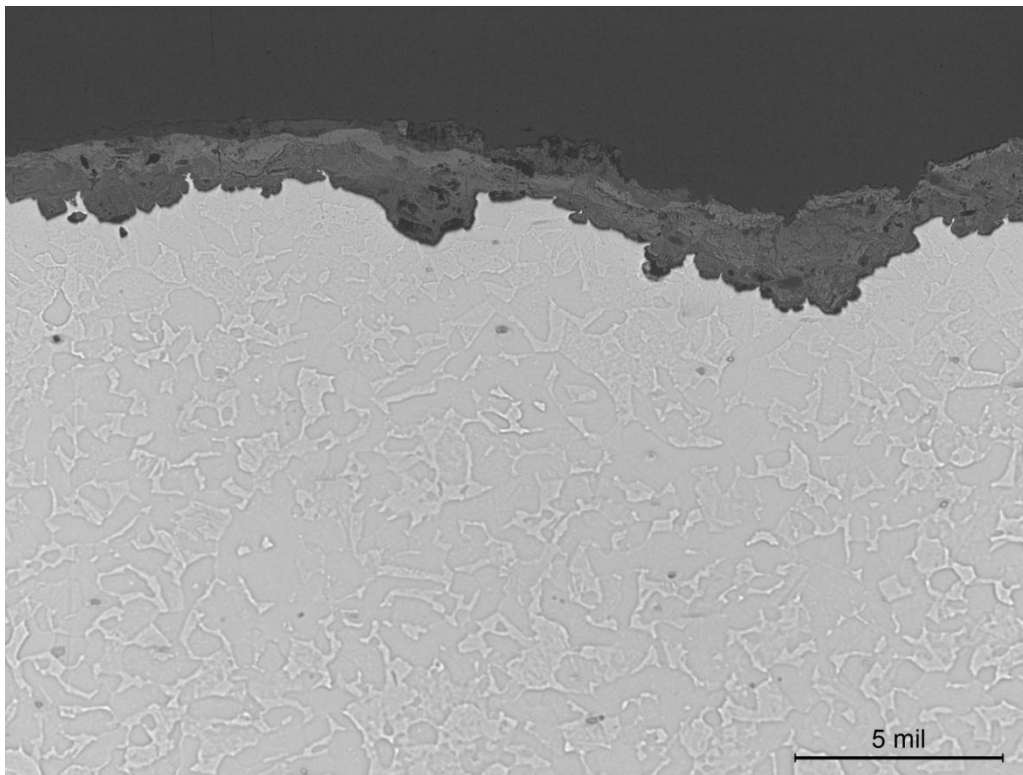
200X

Figure 14 Photograph and micrograph of the floor pit specimen, as-polished.



(a) Boxed area B in Figure 14a

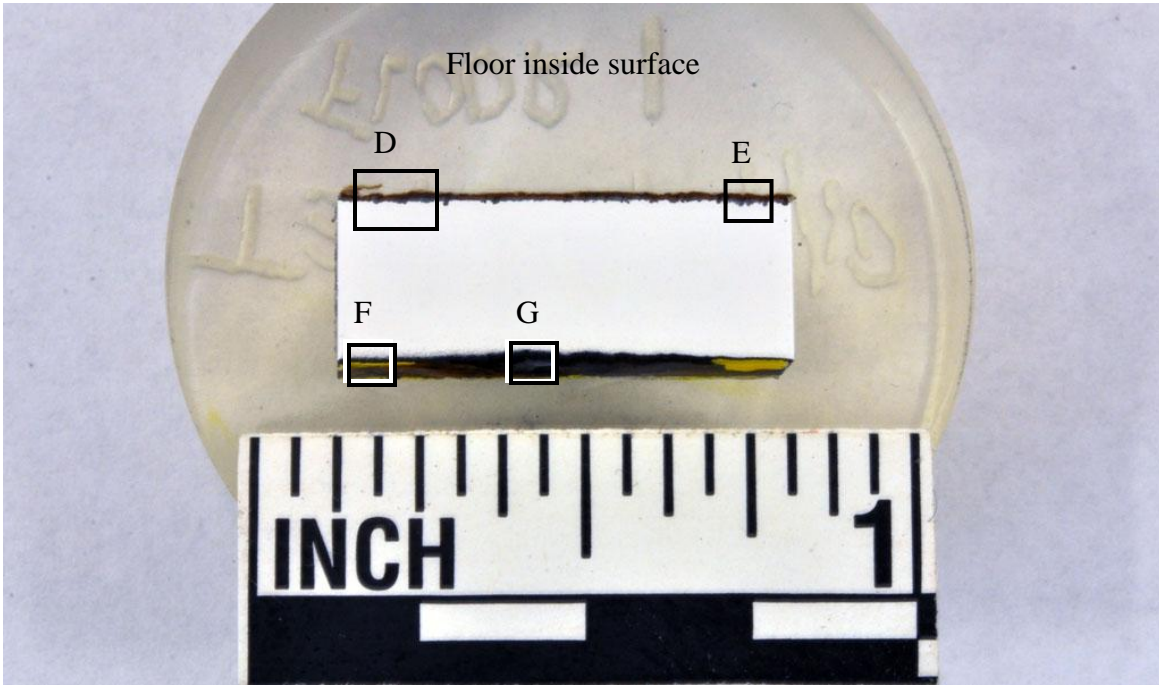
200X



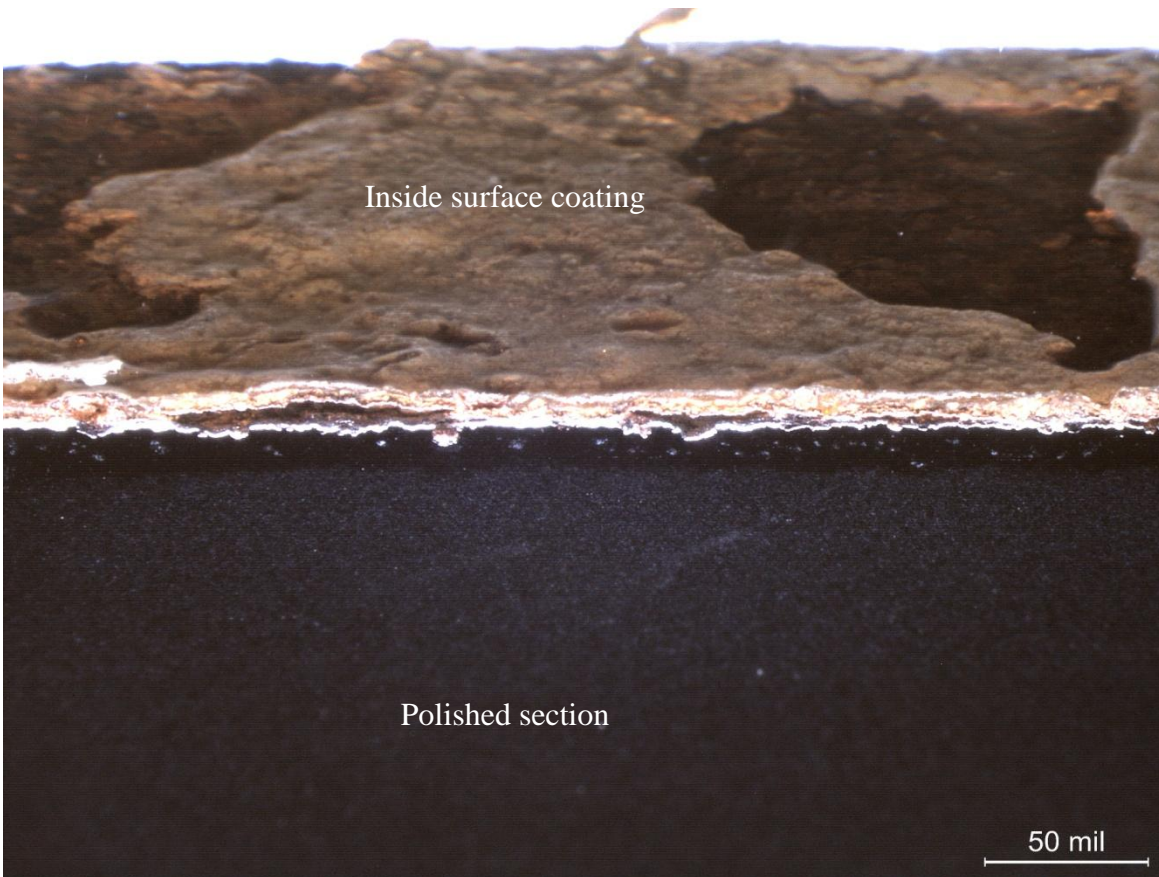
(b) Boxed area C in Figure 14a

200X

Figure 15 Optical micrographs of the floor pit specimen.

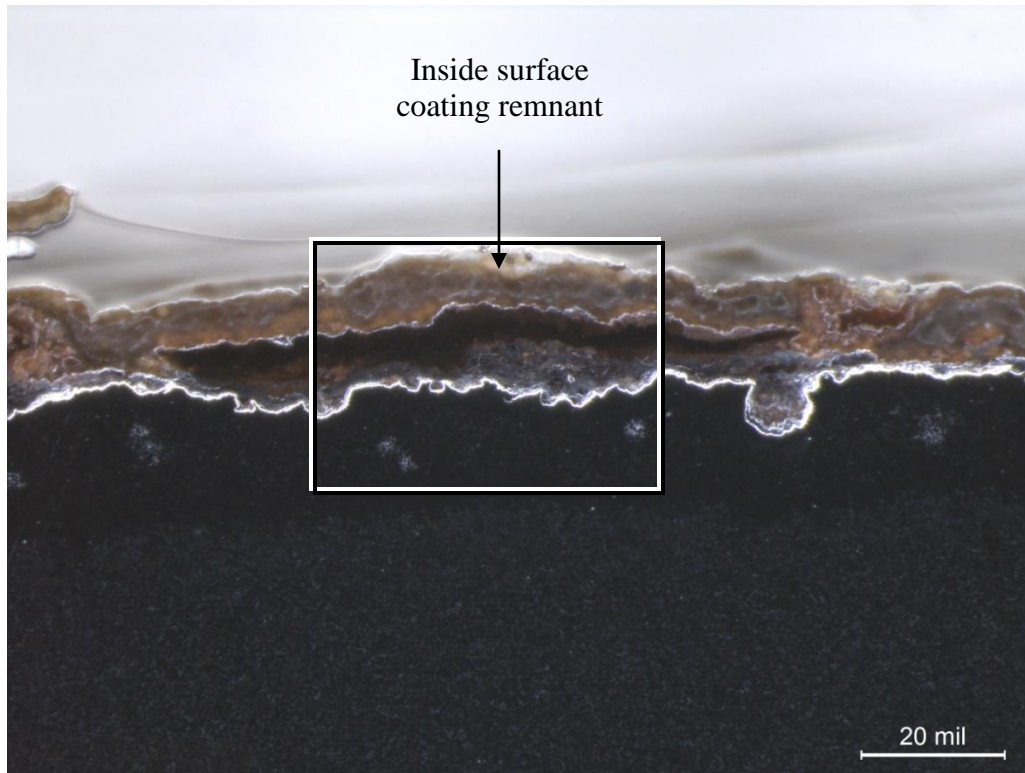


(a) Specimen floor 1



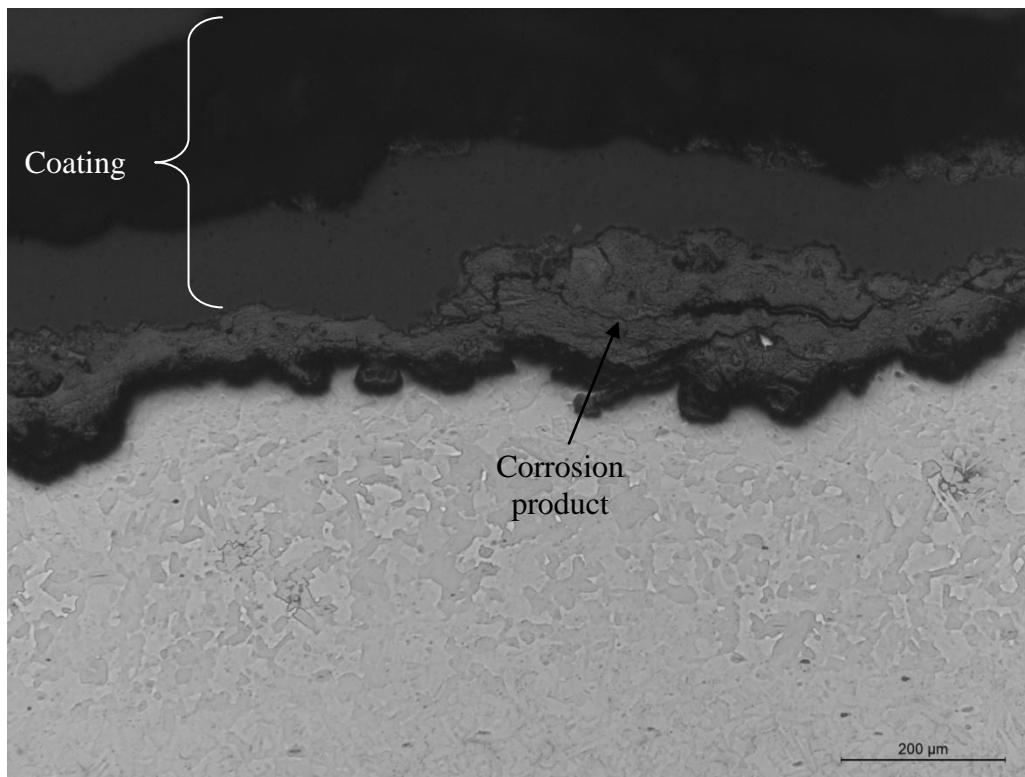
(b) Boxed area D in (a)

Figure 16 Photograph and macrograph of specimen floor 1. In (b) the specimen is viewed at an oblique angle to show the inside surface and the as-polished section.



(a) Boxed area E in Figure 16a

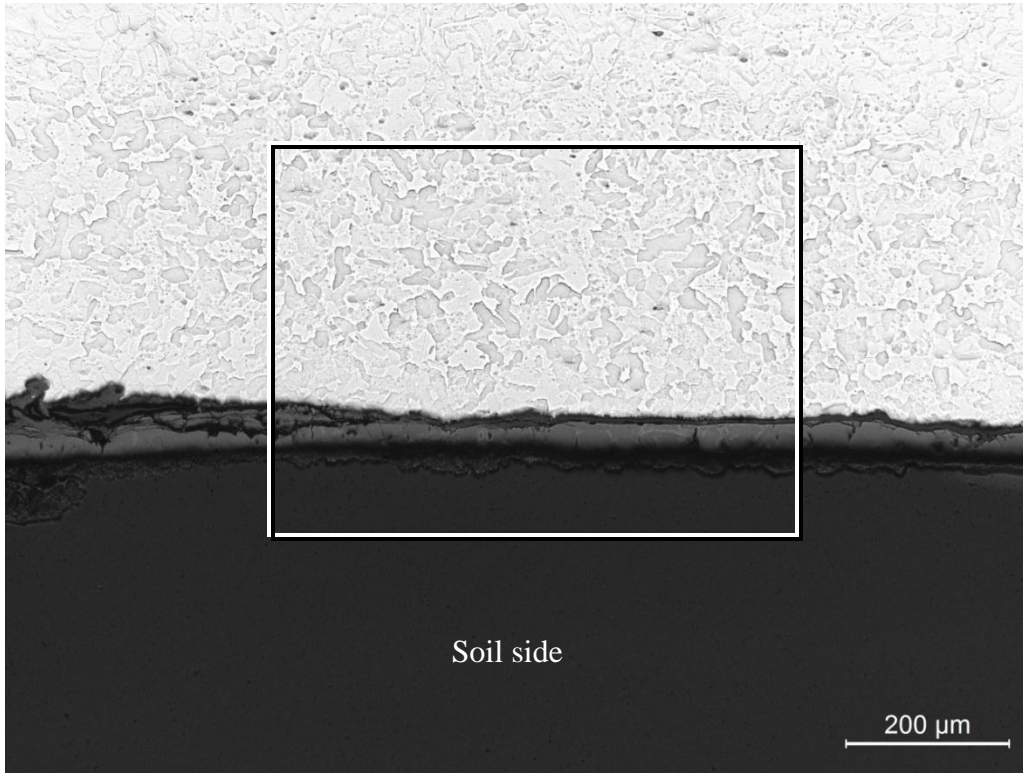
40X



(b) Boxed area in (a)

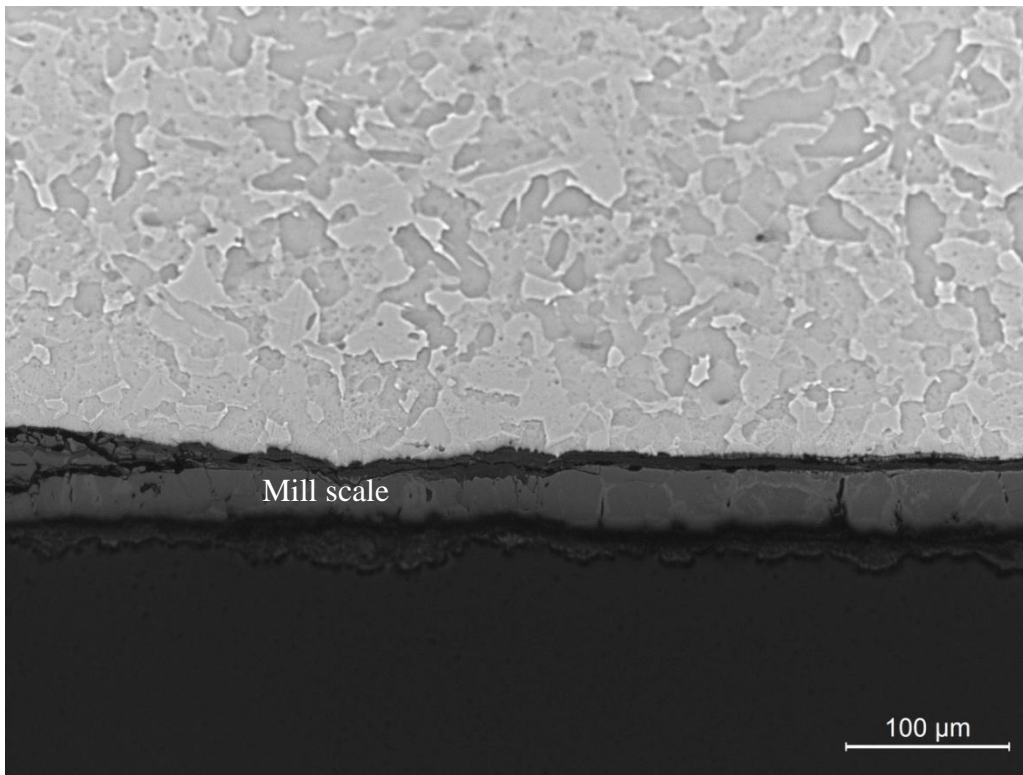
100X

Figure 17 Macrograph and micrograph of specimen floor1 from the boxed area E in Figure 16a.



(a) Boxed area F in Figure 16a

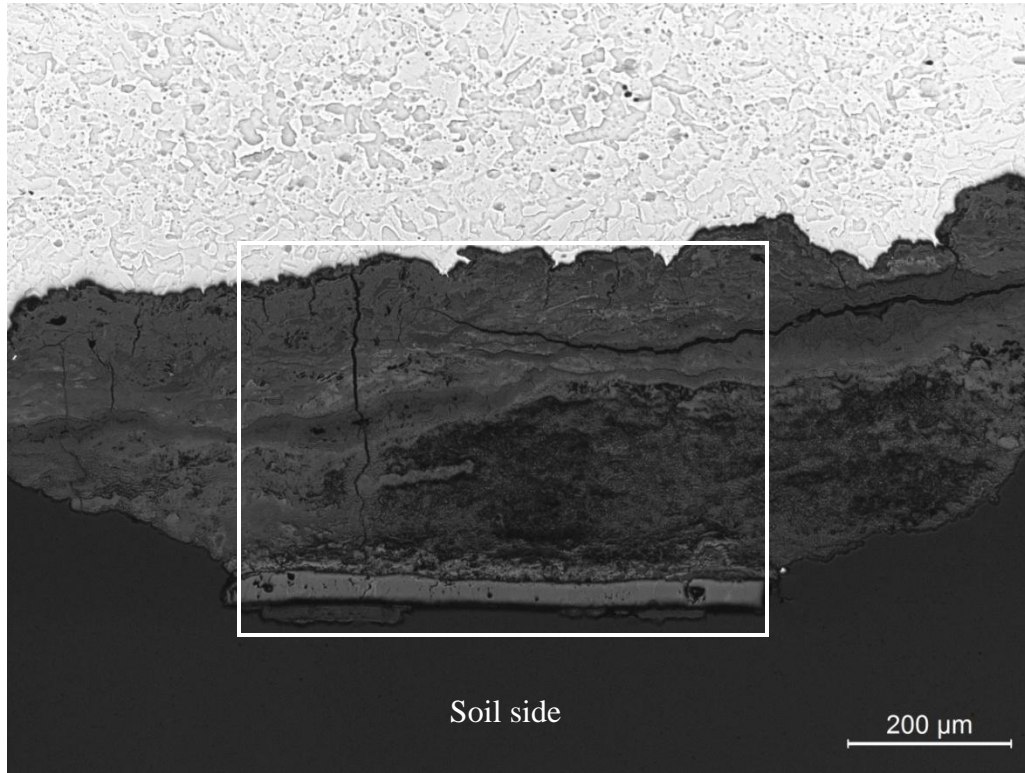
100X



(b) Boxed area in (a)

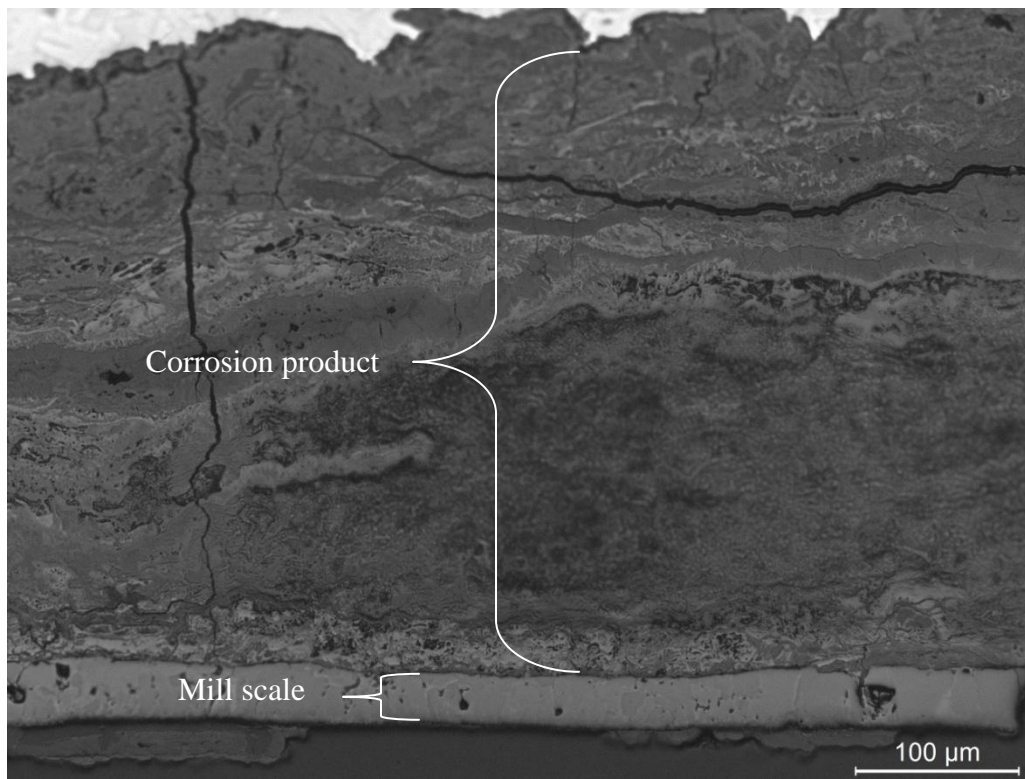
200X

Figure 18 Optical micrographs of the floor 1 specimen from the boxed area F in Figure 16a.



(a) Boxed area G in Figure 15a

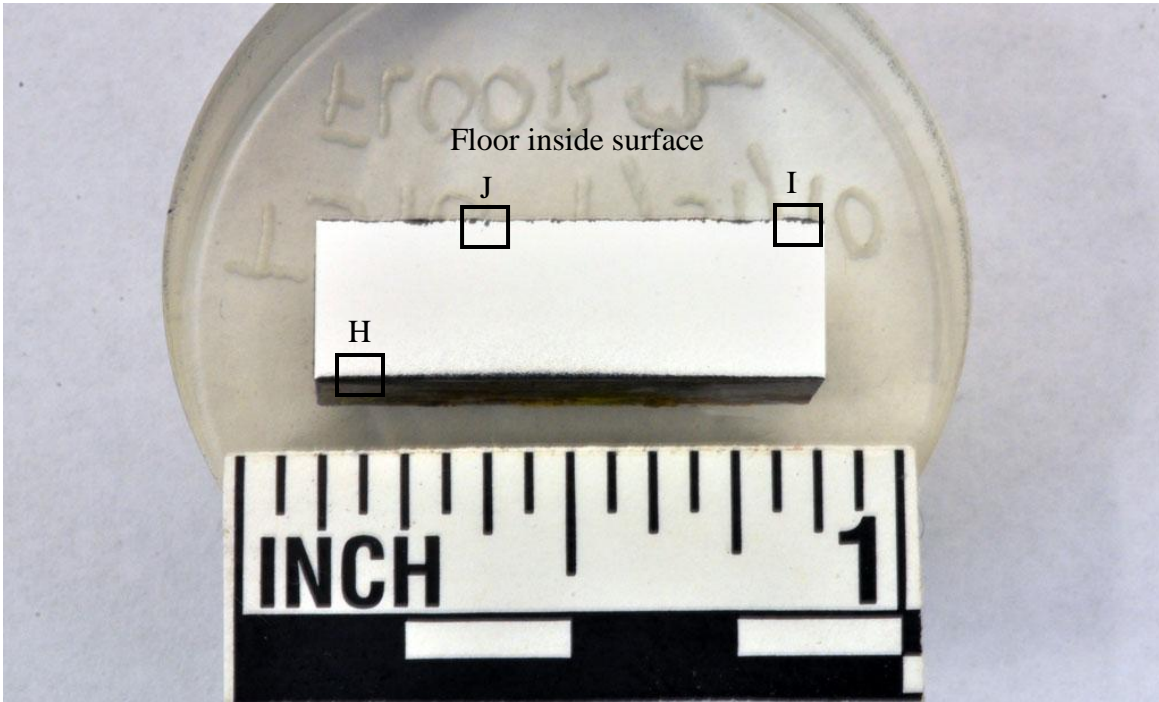
100X



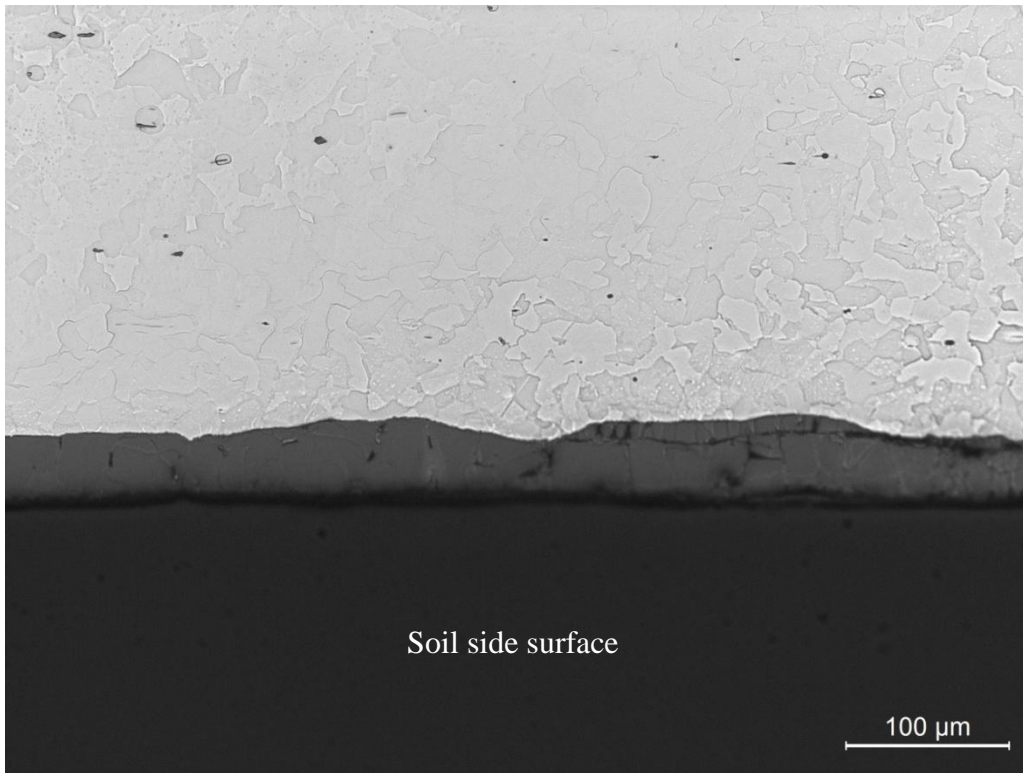
(b) Boxed area in (a)

200X

Figure 19 Optical micrographs of the floor 1 specimen the boxed area G in Figure 16a.



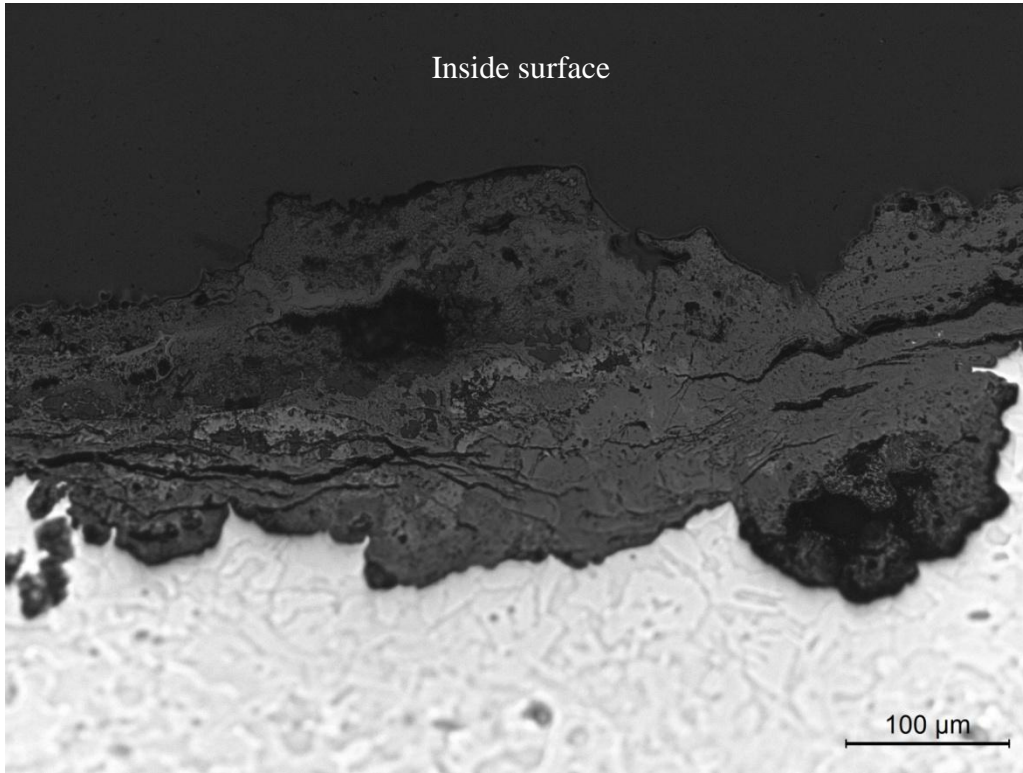
(a) Specimen floor 2



(b) Boxed area H in (a)

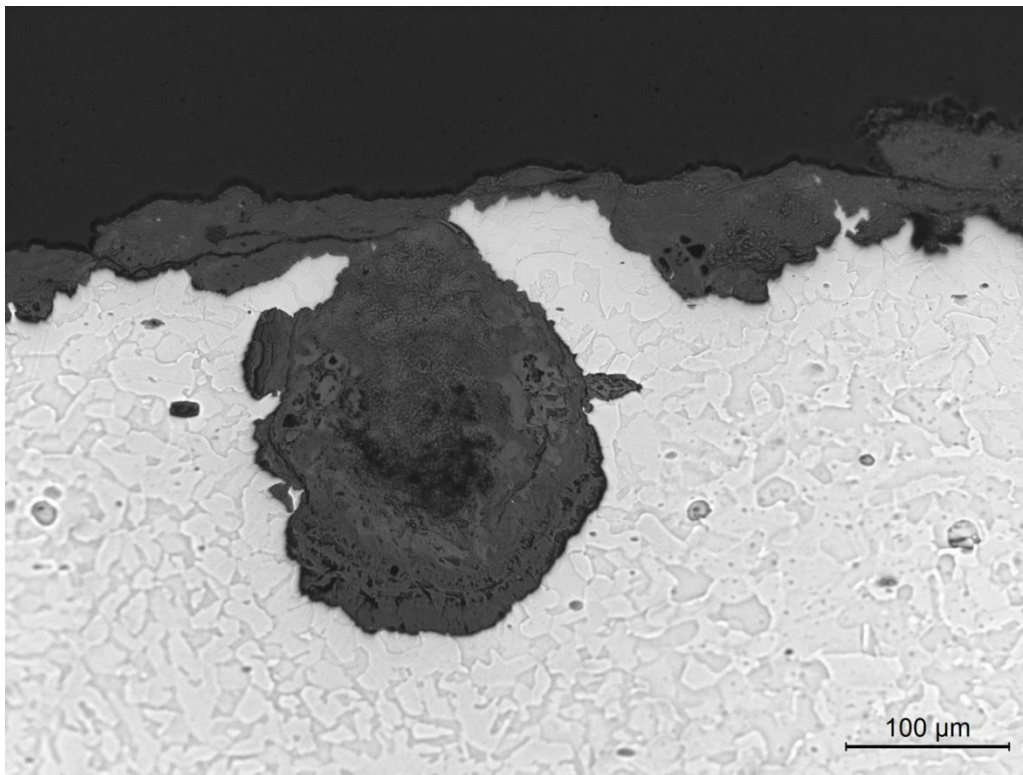
200X

Figure 20 Photograph and optical micrograph of specimen floor 2, as-polished.



(a) Boxed area I in Figure 20a

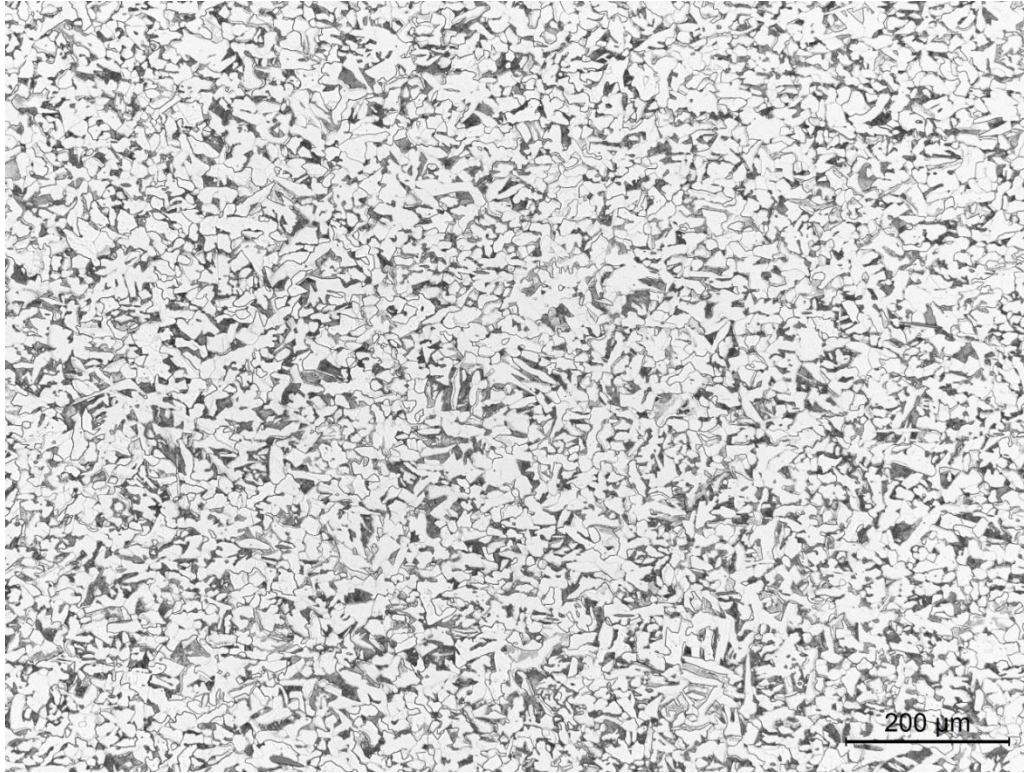
200X



(b) Boxed area J in Figure 20a

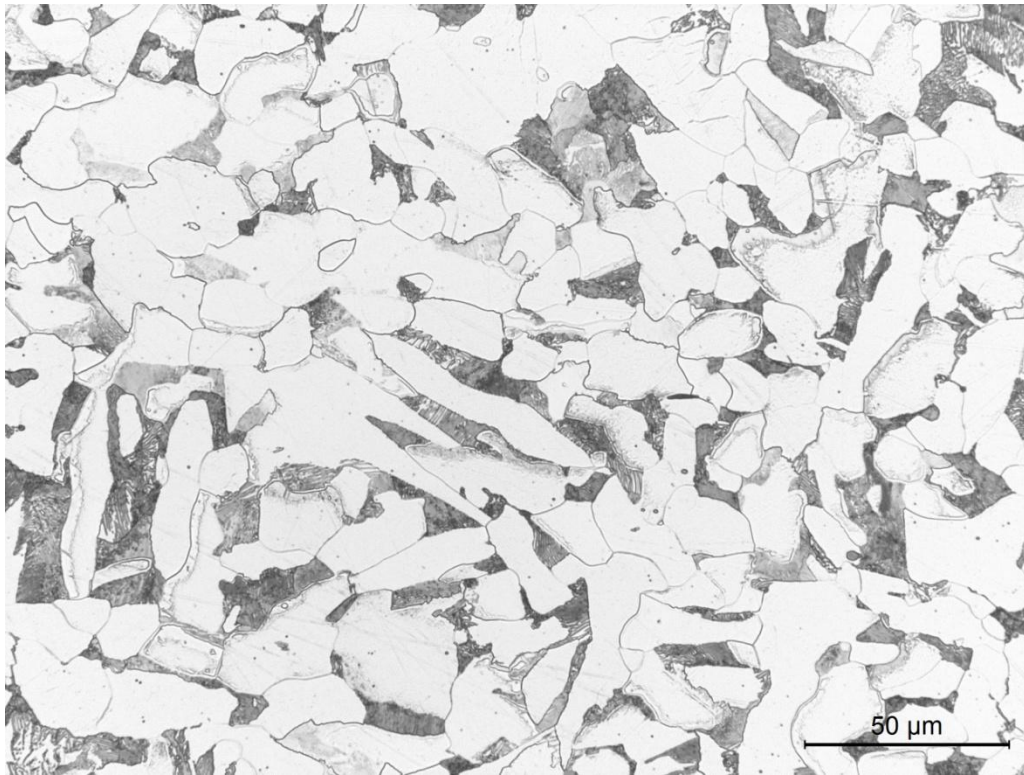
200X

Figure 21 Optical micrographs of specimen floor 2 from the boxed areas I and J in Figure 20a.



(a)

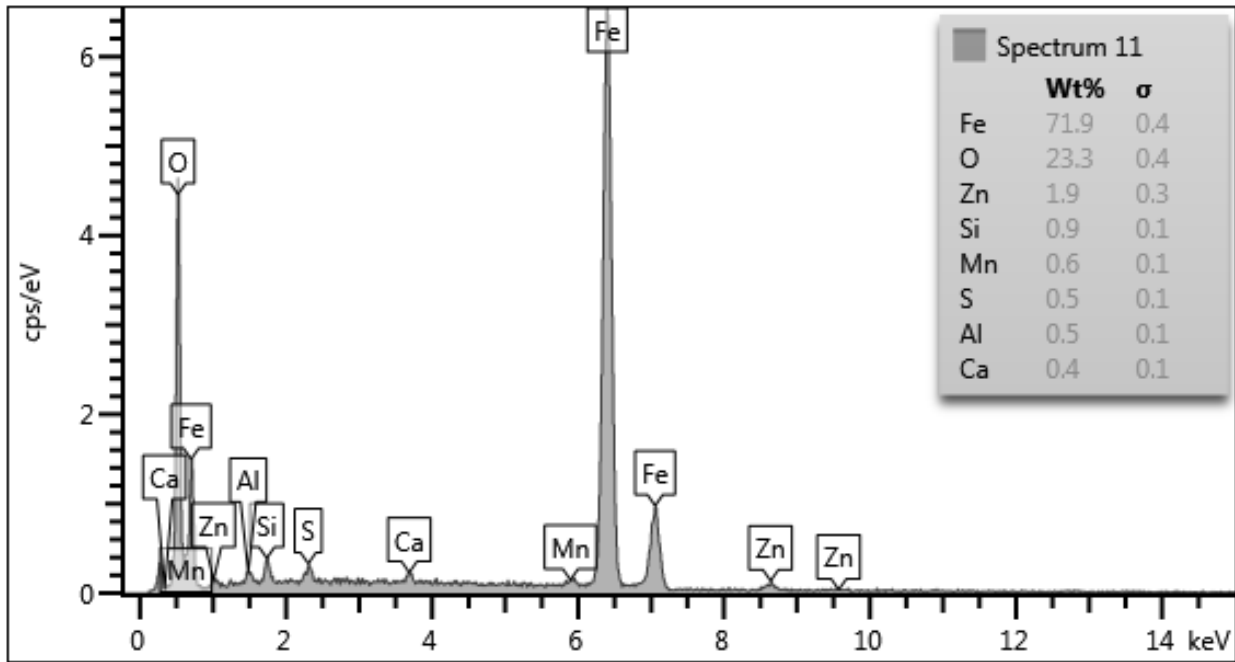
100X



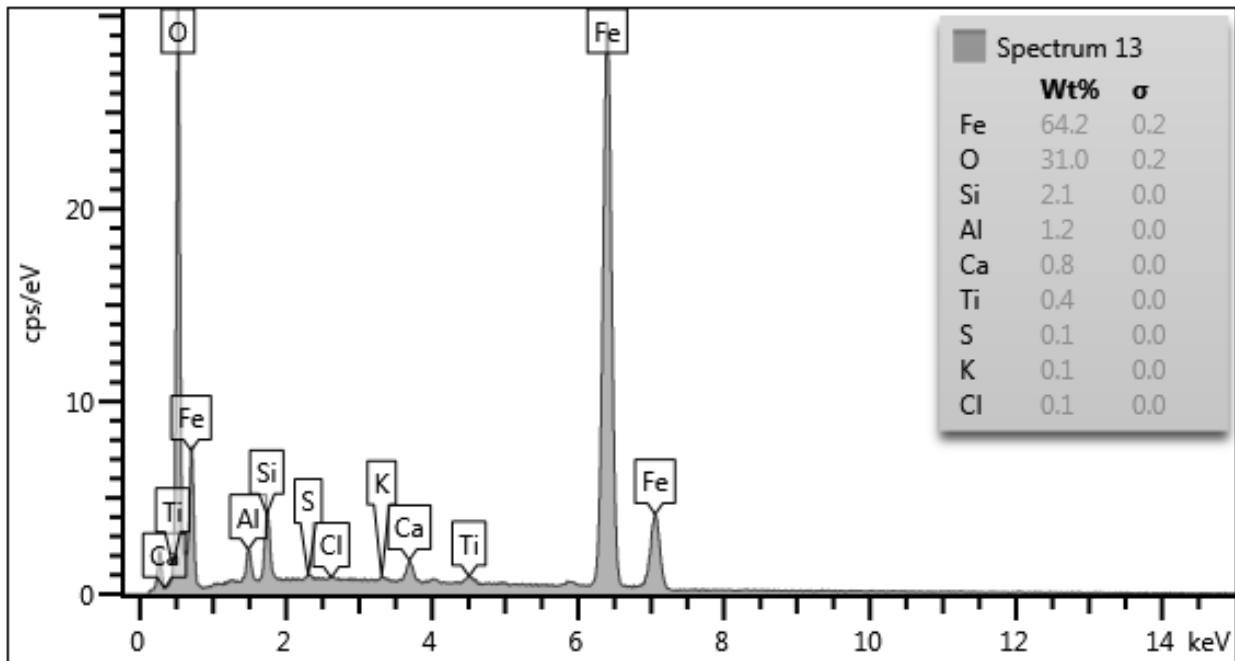
(b)

500X

Figure 22 Optical micrographs of specimen floor 2, etched with 2% nital.



(a) Location 1, Spectrum 11



(b) Location 2, Spectrum 13

Figure 23 EDS spectra from the inside surface of the floor pit at the locations indicated in Figure 13b.

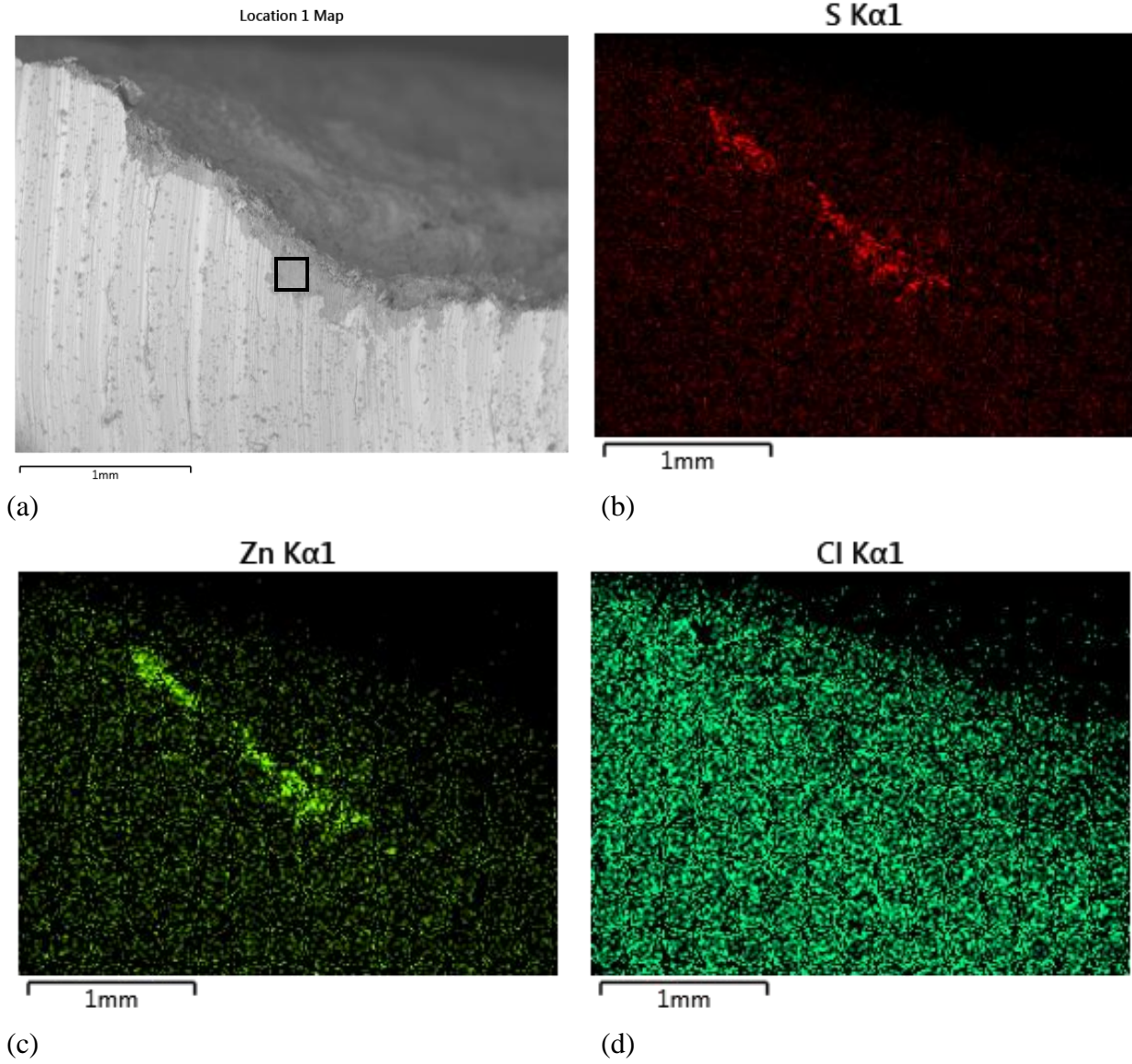
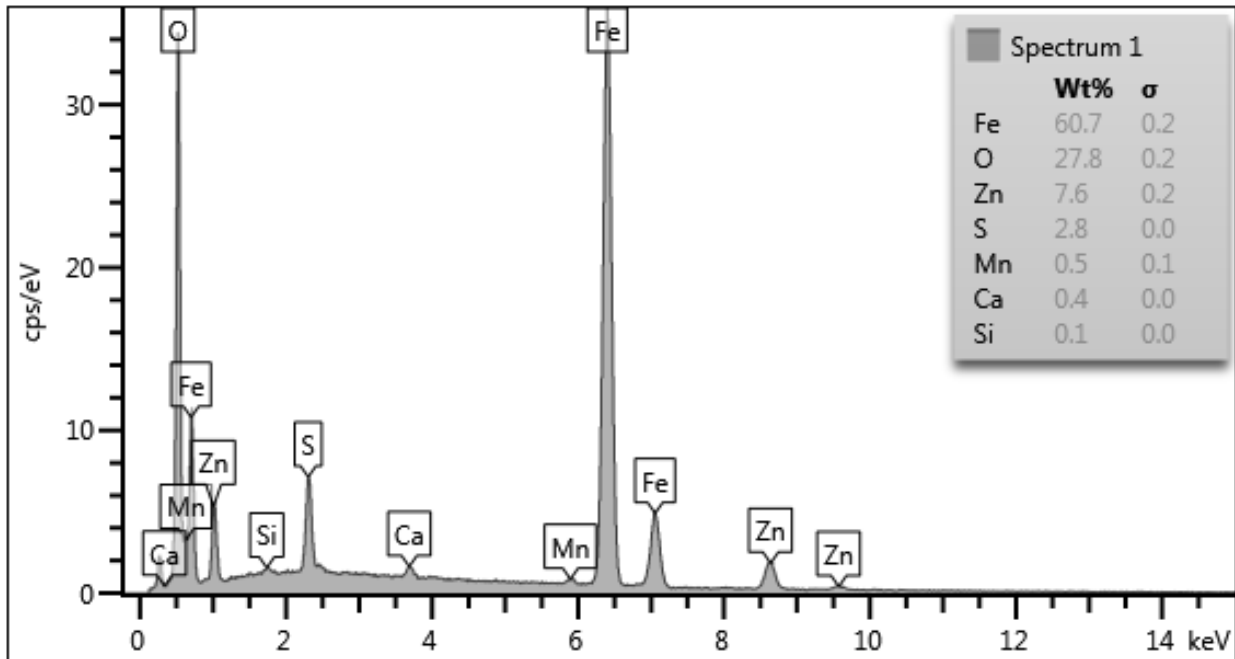
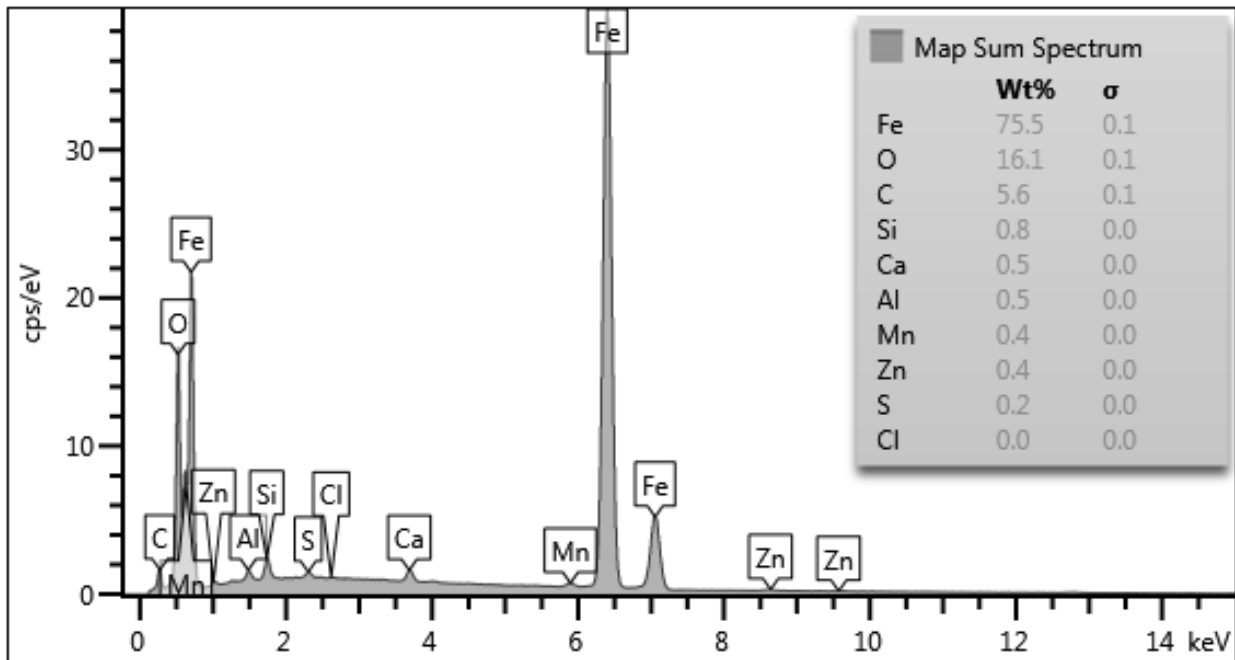


Figure 24 SEM image and EDS maps of the floor pit cross section in the as-cut condition.



(a) Spectrum from boxed area in Figure 24a.



(b) Sum spectrum from the area shown in Figure 24a

Figure 25 EDS spectra from the cross section location shown in Figure 24.

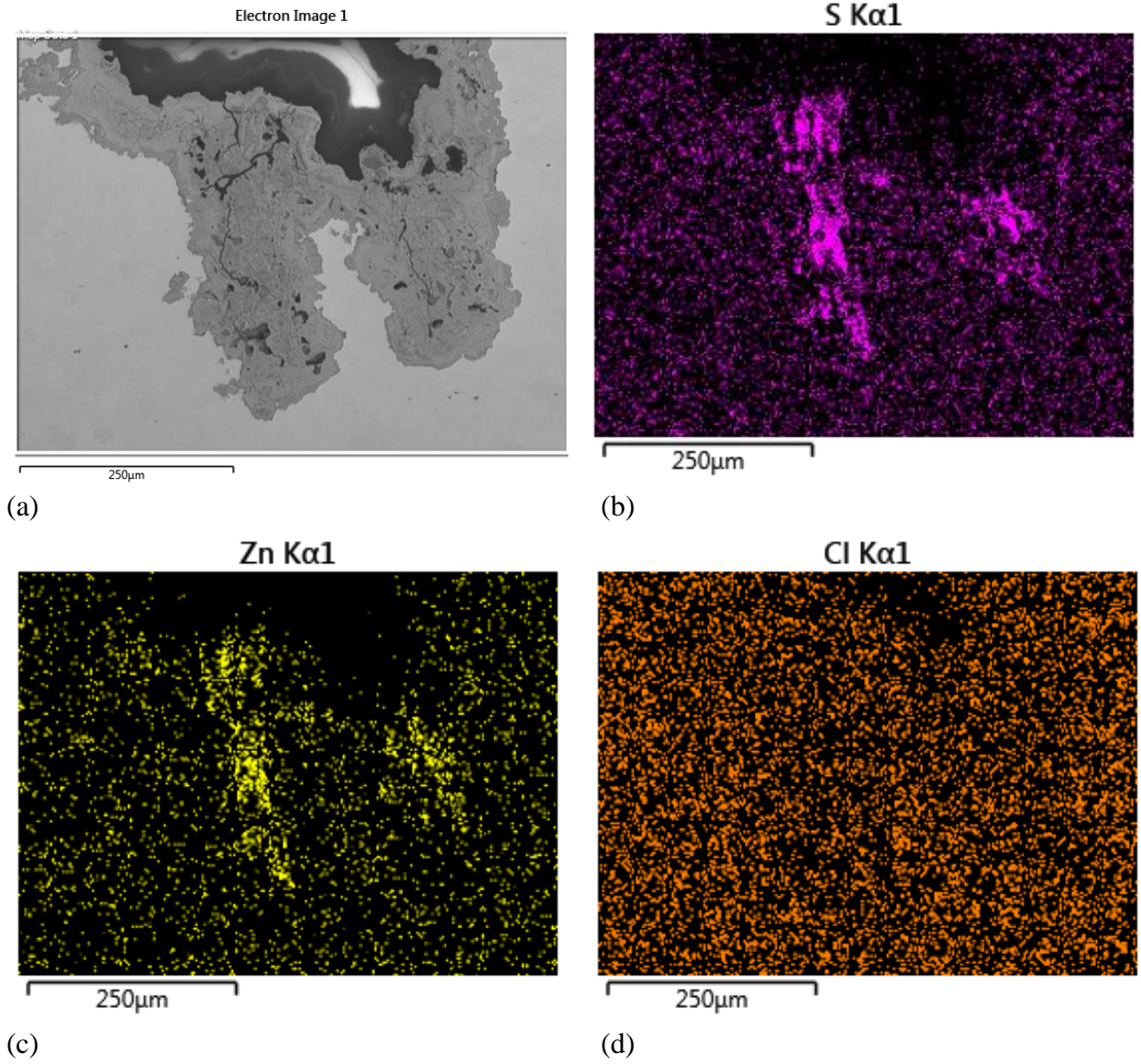


Figure 26 EDS maps from the as-polished specimen floor pit, location shown in Figure 15a.

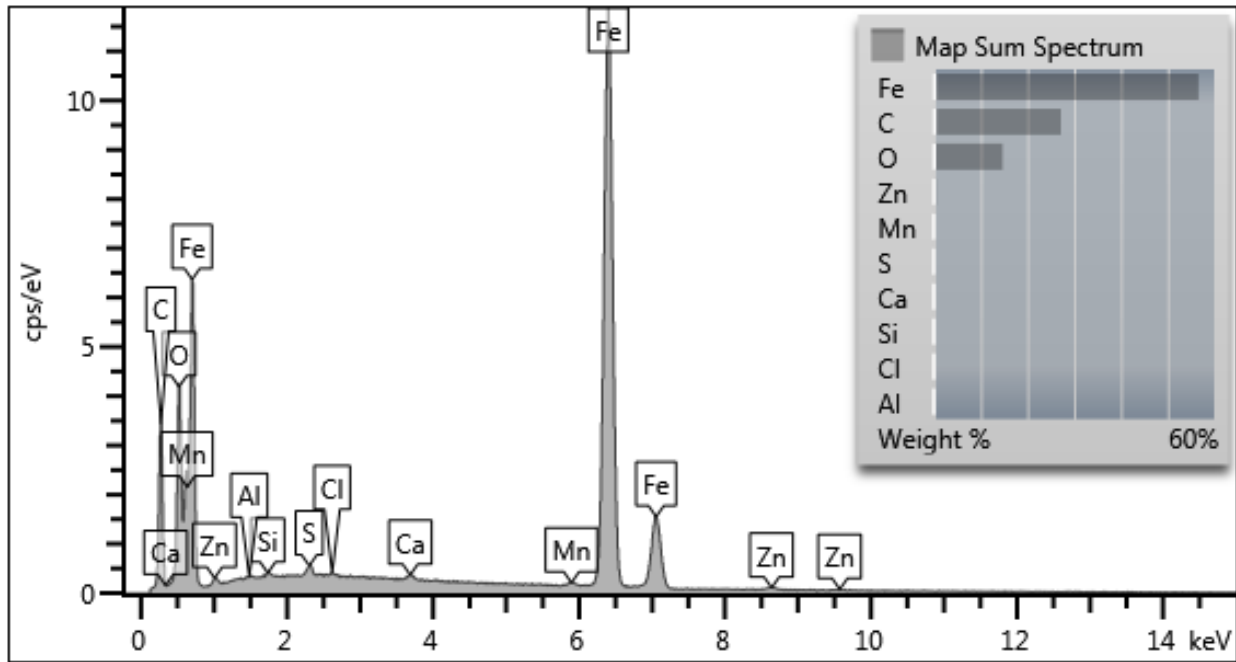


Figure 27 EDS sum spectrum from the as-polished specimen floor pit area mapped in Figure 26.

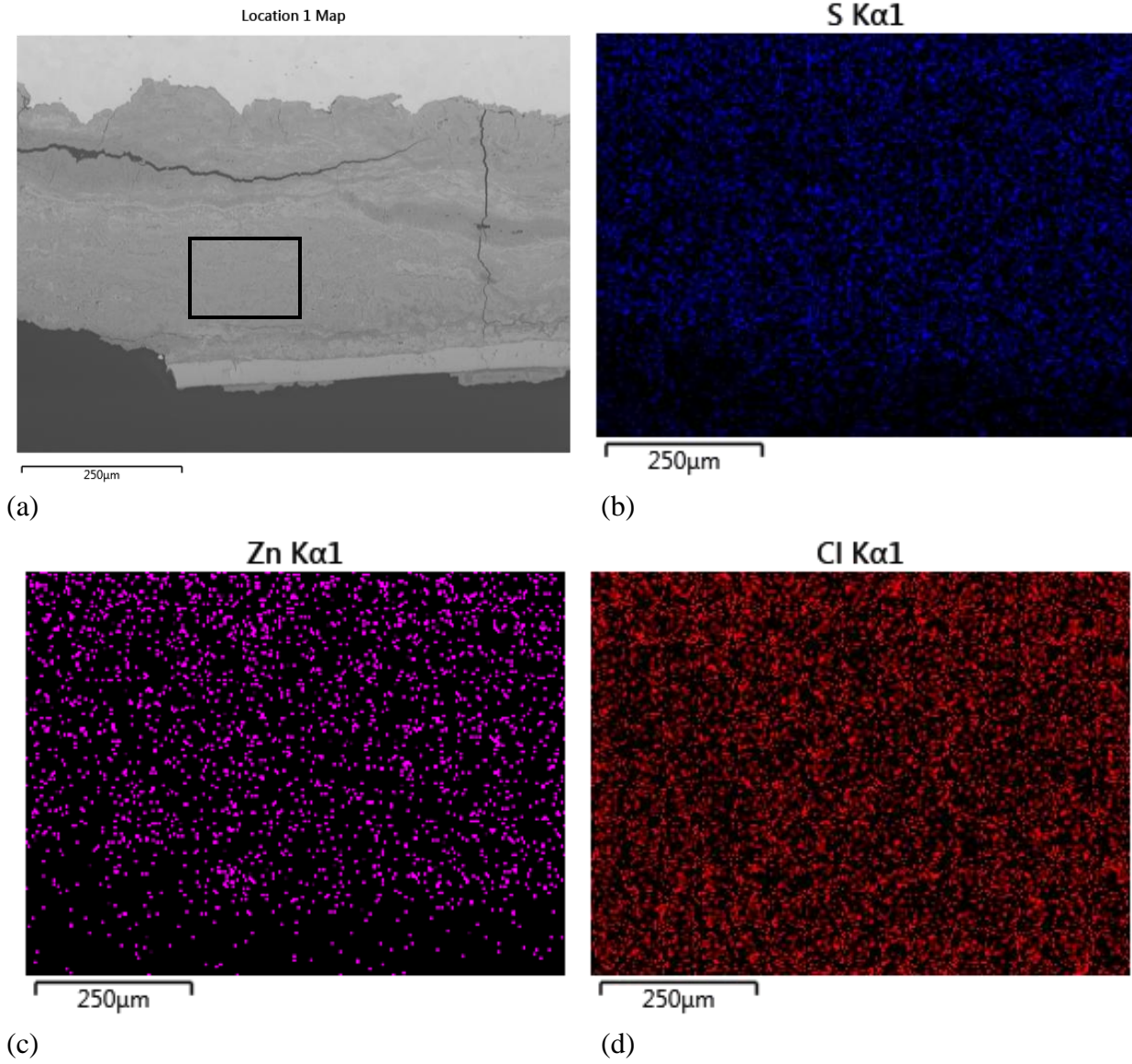
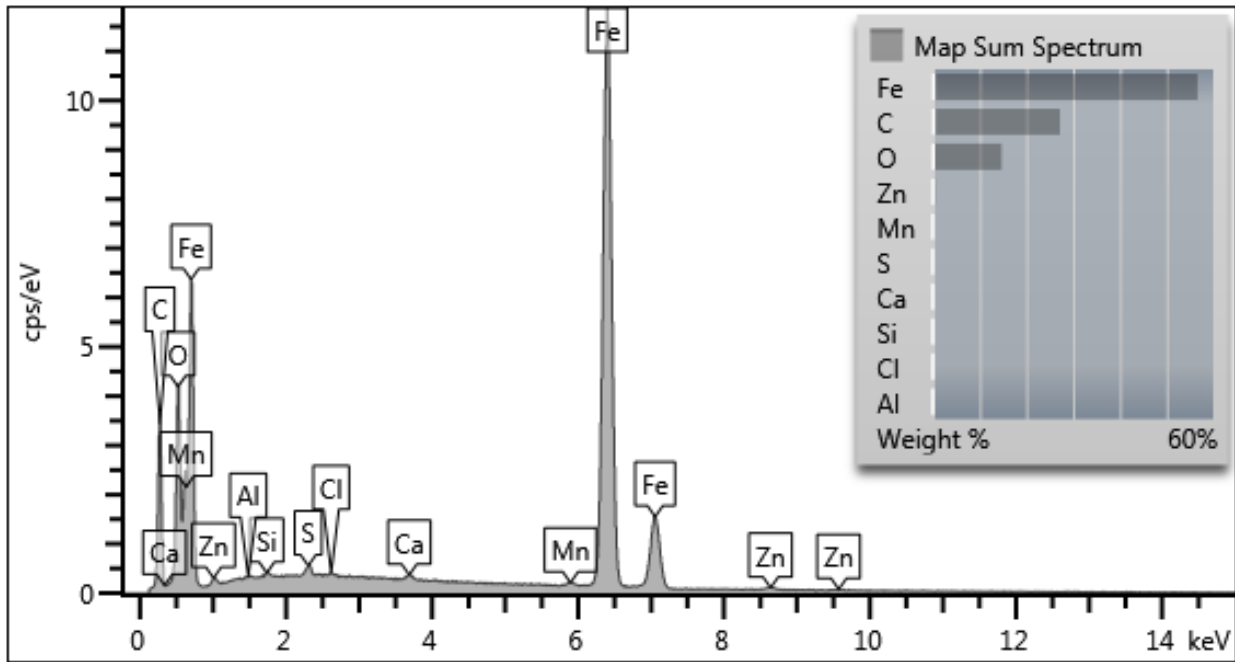
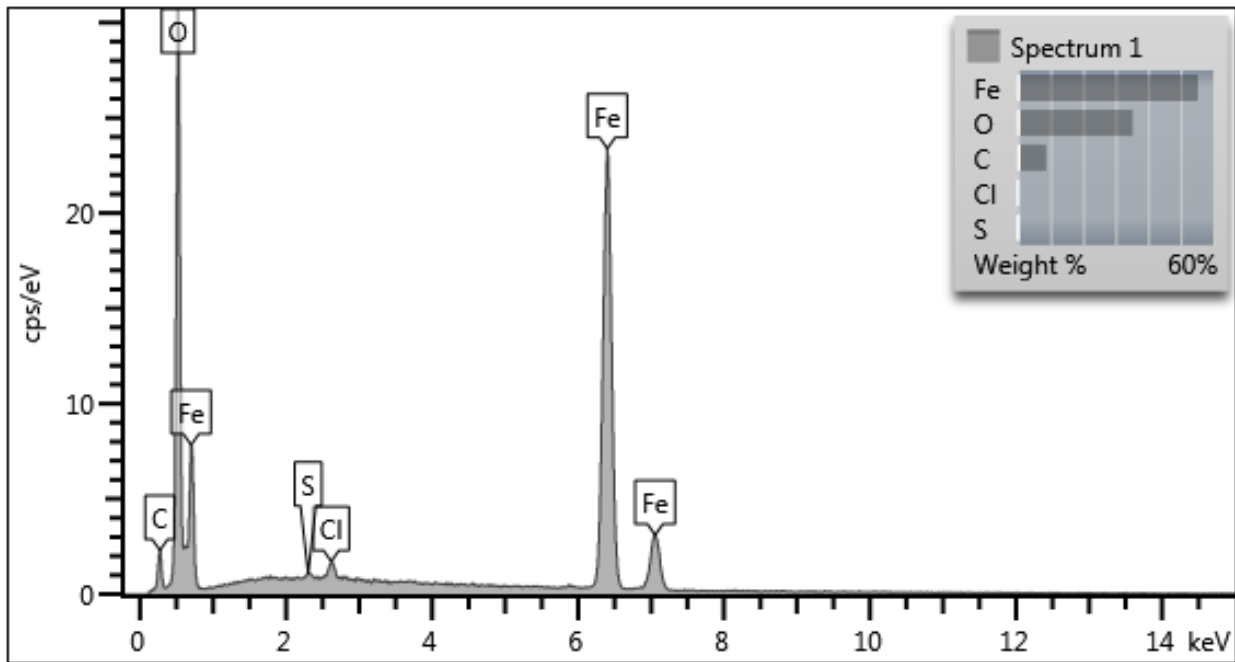


Figure 28 EDS maps from the floor 1 specimen area indicated in Figure 19a.

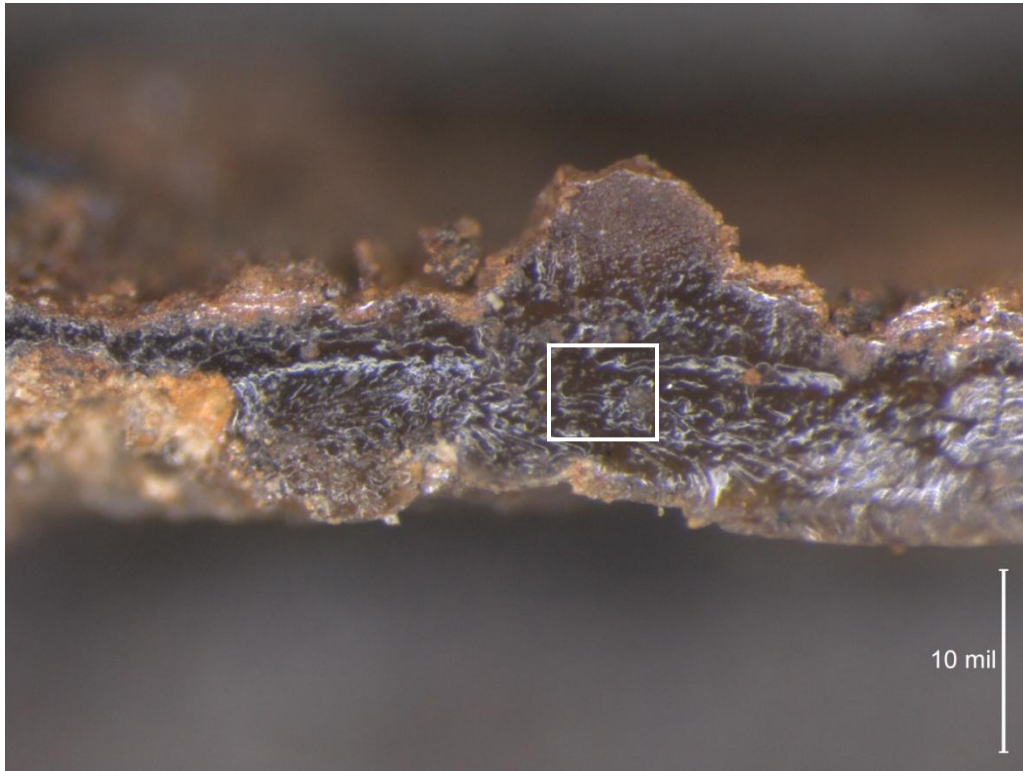


(a) Sum spectrum from the mapped area shown in Figure 28



(b) Spectrum from the boxed area in Figure 28

Figure 29 EDS spectra from the as-polished floor 1 specimen.

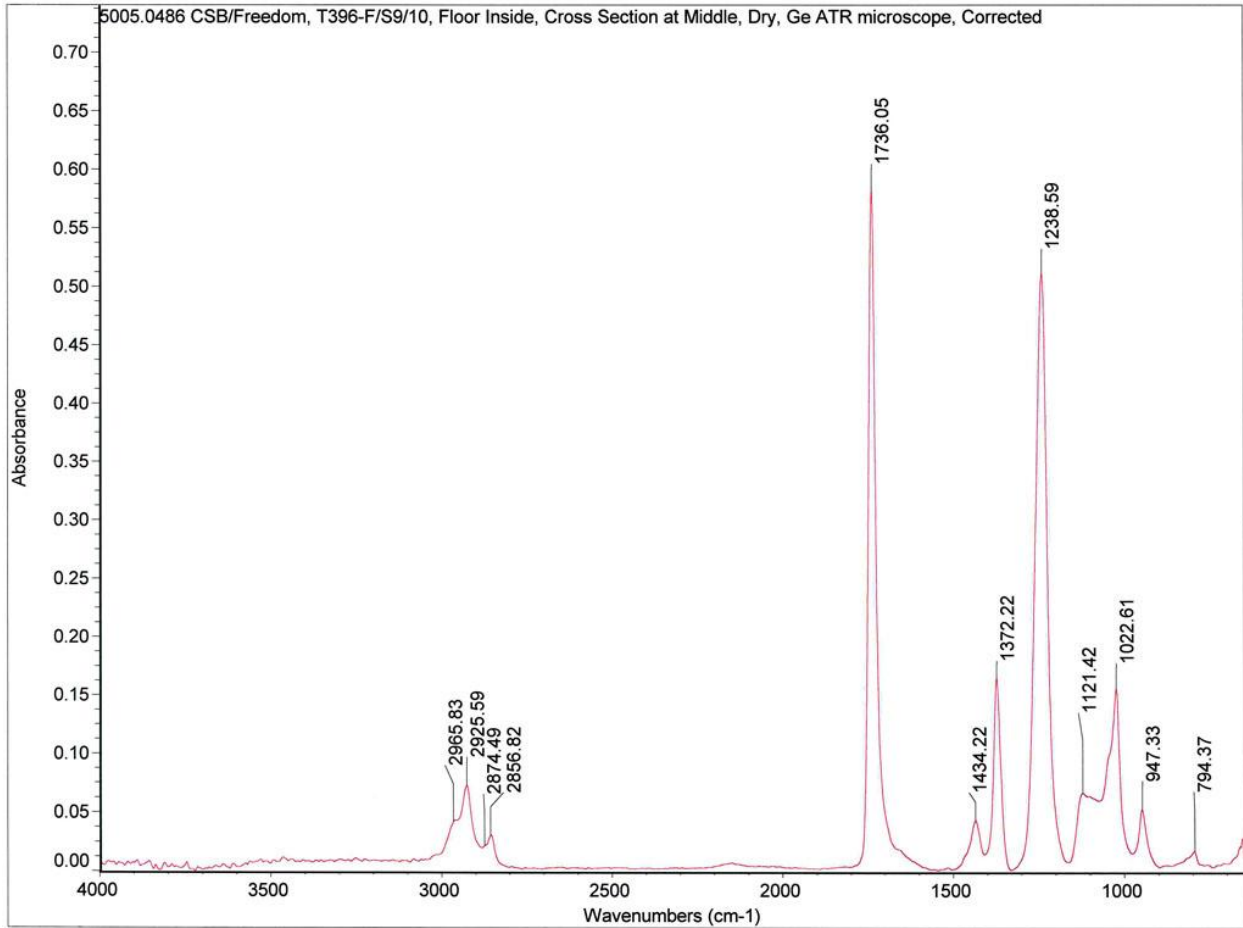


(a)

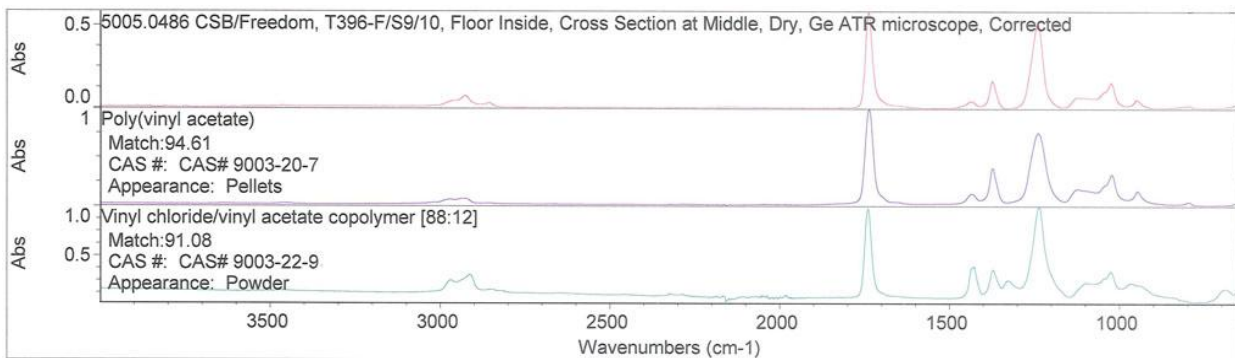


(b)

Figure 30 Cross sections of floor inside surface coating.



(a) Spectrum



(b) Spectrum in (a) compared to two best library matches

Figure 31 FTIR results for the floor inside surface coating.

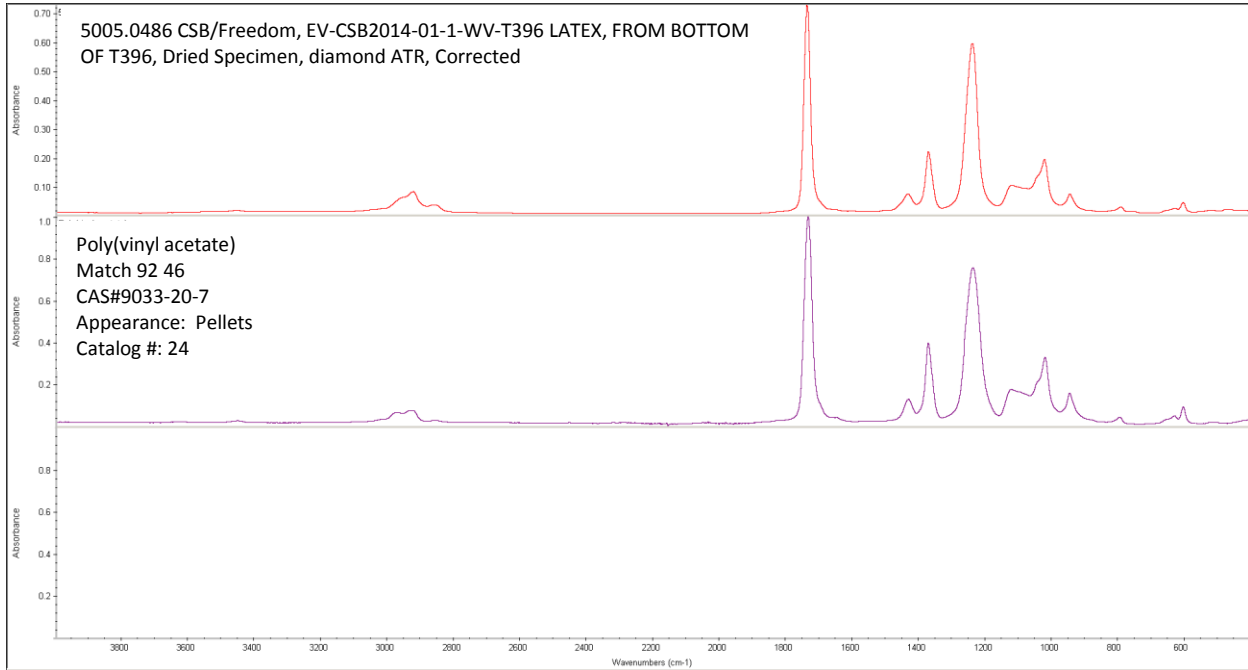
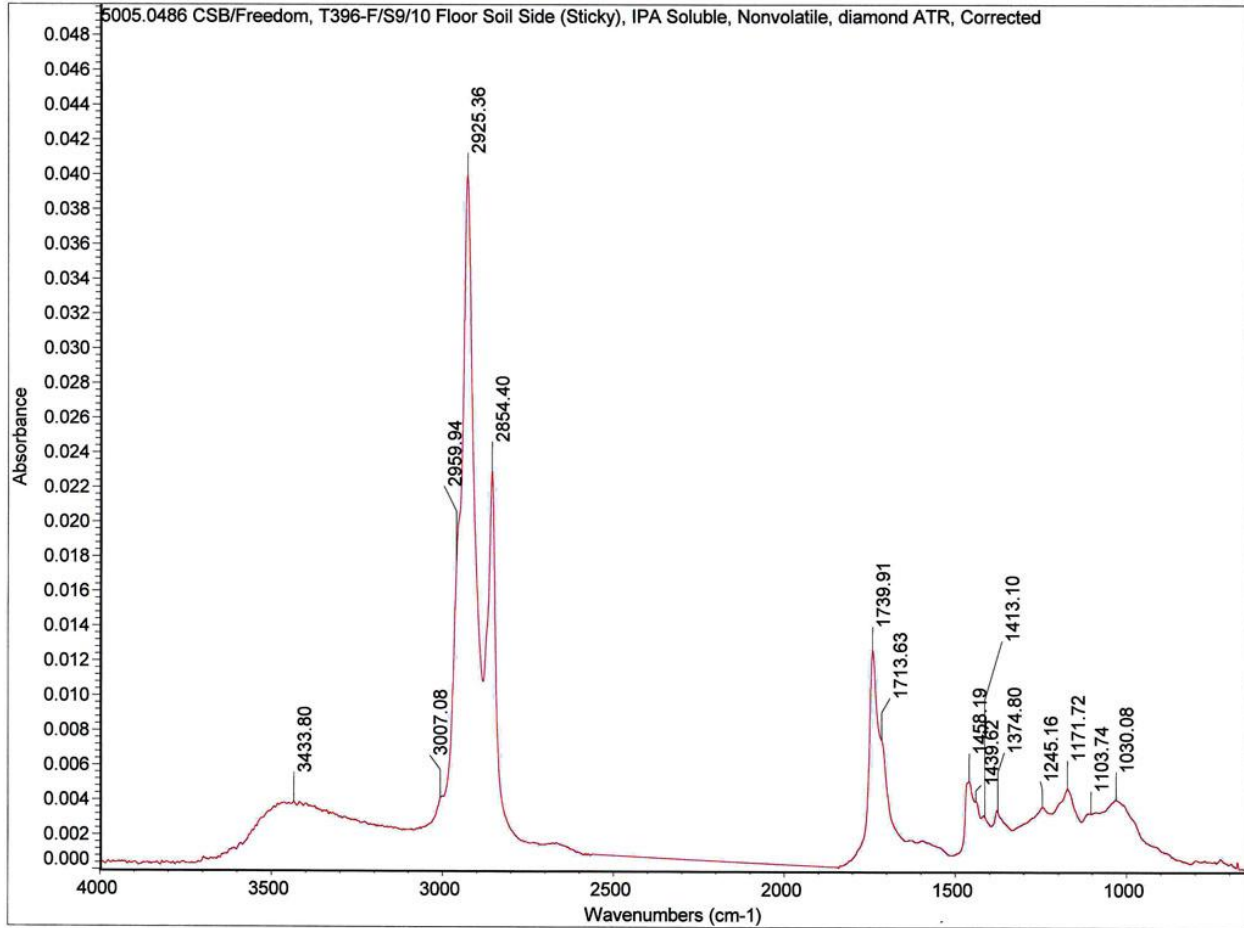
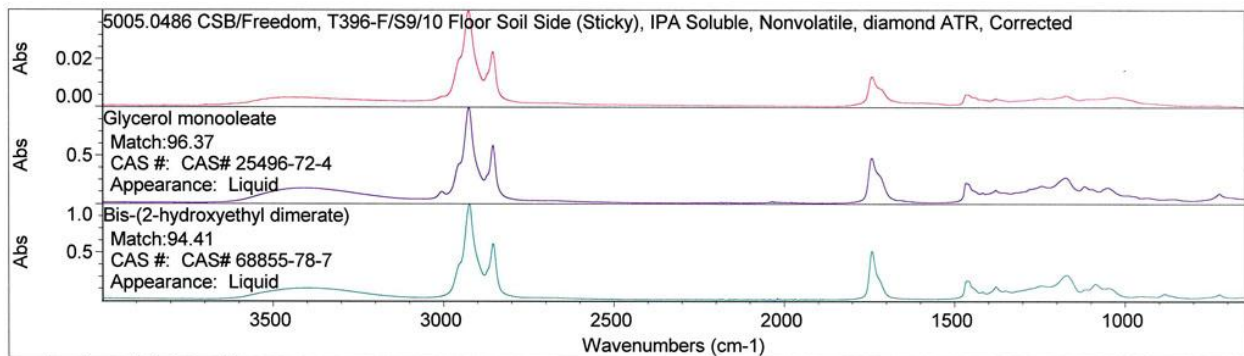


Figure 32 FTIR absorption spectrum and spectrum library match for a specimen of sample labeled EV-CSB2014-01-1-WV-T396 LATEX, FROM BOTTOM OF T396. The specimen spectrum and match were the same as for specimens from the T396-F/S9/10 floor inside surface coating.



(a) Spectrum



(b) Spectrum in (a) compared to two best library matches

Figure 33 FTIR results for the sticky soil side floor specimen.



Appendix



Testing Cert. #2797.01

**X-RAY DIFFRACTION (XRD)  
ANALYSIS REPORT  
24 Oct 2014**

**JOB NUMBER C0ENB225  
PO NUMBER 15758**

for

Sam McFadden  
Anamet, Inc.  
26102 Eden Landing Rd. Ste 3  
Hayward, CA 94545

Prepared by:

---

Bich Nguyen  
Senior Analyst, XRD Services  
(Tel. 408-530-3834; [bnguyen@eag.com](mailto:bnguyen@eag.com))

Reviewed by:

---

Stephen B. Robie, Ph.D.  
Specialist, XRD Services  
(Tel. 408-530-3638; [srobie@eag.com](mailto:srobie@eag.com))

Evans Analytical Group  
810 Kifer Rd  
Sunnyvale, CA 94086 USA



Appendix

Requester: Sam McFadden  
Job Number: C0ENB225  
Analysis Date: 24 Oct 2014

**X-RAY DIFFRACTION ANALYSIS REPORT**

**Purpose:** Use x-ray diffraction to determine the phases present in four corrosion products scraped from carbon steel. The samples were identified as indicated in the table below.

**Summary:**

**Best Matches from the ICDD/ICSD data bases**

Sample ID	Primary Phases	Minor or Possible Trace Phases
<p><b>Sample 1</b> <b>(Floor inside surface #1)</b></p>	<p>Fe<sub>2</sub>O<sub>3</sub> – Maghemite-C Cubic P4132 PDF# 00-039-1346</p>	<p>α-Fe<sup>+3</sup>O(OH) – Goethite Orthorhombic Pbnm PDF# 00-029-0713</p> <p>γ-Fe<sup>+3</sup>O(OH) – Lepidocrocite Orthorhombic Bbmm PDF# 00-044-1415</p> <p>Mg<sub>3</sub>Fe<sub>2</sub>(SiO<sub>4</sub>)<sub>3</sub> – Majorite Tetragonal I41/a PDF# 00-025-0843</p> <p>SiO<sub>2</sub> – Quartz Hexagonal P3221 PDF# 00-046-1045</p> <p>CaCO<sub>3</sub> – Calcite Hexagonal R-3c PDF# 00-005-0586</p>
<p><b>Sample 2</b> <b>(Floor inside surface #2)</b></p>	<p>Mg<sub>3</sub>Fe<sub>2</sub>(SiO<sub>4</sub>)<sub>3</sub> – Majorite Tetragonal I41/a PDF# 00-025-0843</p> <p>SiO<sub>2</sub> – Quartz Hexagonal P3221 PDF# 00-046-1045</p>	<p>Fe<sub>2</sub>O<sub>3</sub> – Maghemite-C Cubic P4132 PDF# 00-039-1346</p> <p>α-Fe<sup>+3</sup>O(OH) – Goethite Orthorhombic Pbnm PDF# 00-029-0713</p> <p>γ-Fe<sup>+3</sup>O(OH) – Lepidocrocite Orthorhombic Bbmm PDF# 00-044-1415</p> <p>CaCO<sub>3</sub> – Calcite Hexagonal R-3c PDF# 00-005-0586</p>



Appendix

XRD Analysis Report  
EAG Number C0ENB225  
Sam McFadden  
Anamet, Inc.

Page 3 of 10  
24 Oct 2014

<p><b>Sample 3</b> (Floor soil side #1)</p>	<p><math>\alpha\text{-Fe}^{+3}\text{O(OH)}</math> – Goethite Orthorhombic Pbnm PDF# 00-029-0713</p> <p><math>\text{Fe(CO}_3\text{)}</math> – Siderite Hexagonal R-3c PDF# 04-015-9760</p>	<p><math>\text{CaCO}_3</math> – Calcite Hexagonal R-3c PDF# 00-005-0586</p> <p><math>\text{Fe}_2\text{O}_3</math> – Maghemite-C Cubic P4132 PDF# 00-039-1346</p> <p><math>\text{Fe}_{9.5}\text{O}_{14}(\text{OH})_2</math> – Ferrihydrite Hexagonal P63mc PDF# 00-058-0900</p> <p><math>\text{SiO}_2</math> – Quartz Hexagonal P3221 PDF# 00-046-1045</p> <p>Unknown phase(s)</p>
<p><b>Sample 4</b> (Floor soil side #2)</p>	<p><math>\alpha\text{-Fe}^{+3}\text{O(OH)}</math> – Goethite Orthorhombic Pbnm PDF# 00-029-0713</p> <p><math>\text{Fe(CO}_3\text{)}</math> – Siderite Hexagonal R-3c PDF# 04-015-9760</p>	<p><math>\text{CaCO}_3</math> – Calcite Hexagonal R-3c PDF# 00-005-0586</p> <p><math>\text{Fe}_3\text{O}_4</math> – Magnetite Cubic Fd-3m PDF# 00-019-0629</p> <p><math>\text{Fe}_{9.5}\text{O}_{14}(\text{OH})_2</math> – Ferrihydrite Hexagonal P63mc PDF# 00-058-0900</p> <p><math>\text{SiO}_2</math> – Quartz Hexagonal P3221 PDF# 00-046-1045</p> <p>Unknown phase(s)</p>

**Results and Interpretations:** The samples were prepared by grinding in a mortar and pestle. The resulting powders from each sample were pressed into a bulk sample holder with a glass slide for analysis. XRD data was collected by a coupled Theta:2-Theta scan on a Rigaku Ultima-III diffractometer equipped with a Copper X-ray tube, computer-controlled slits, and D/Tex Ultra 1D strip detector.

Figure 1 compares the XRD raw data from all four samples. There are significant differences between these patterns in terms of overall intensities, peak shape and peak positions.

Figure 2 and Figure 3 shows the best matches between the background-subtracted experimental data to the ICDD/ICSD diffraction database for sample 1 (Floor inside surface #1)



---

## Appendix

XRD Analysis Report  
EAG Number C0ENB225  
Sam McFadden  
Anamet, Inc.

Page 4 of 10  
24 Oct 2014

and sample 2 (Floor inside surface #2). The Maghemite cubic phase is the major phase in sample 1. Majorite and Quartz are the major phases observed in sample 2 while they are detected as minor phases in sample 1. Two polymorphs of Iron Oxy-hydroxide phases (FeO(OH)  $\alpha$  (Goethite) and  $\gamma$  (Lepidocrocite) as well as Calcite are present as trace phases in these two samples as well.

The phase identification results for sample 3 (Floor soil side #1) and sample 4 (Floor soil side #2) are shown in [Figure 4](#) and [Figure 5](#), respectively. Goethite and Siderite are the primary phases in both of these samples. Maghemite is a good match in sample 4 while Magnetite agrees well with most of the minor peaks in sample 3. Calcite is also identified as a minor phase in sample 3 at a greater concentration than in sample 4. Several weak peaks in both samples matched Quartz and Ferrihydrite, but these should be considered speculative matches due to the many peak overlaps present. In addition, there are few weak peaks that could not be matched in both samples.

After reviewing this report, you may assess our services using an electronic service evaluation form. This can be done by clicking on the link below, or by pasting it into your internet browser. Your comments and suggestions allow us to determine how to better serve you in the future.  
<http://www.eaglabs.com/main-survey.html?job=C0ENB225>

**This analysis report should not be reproduced except in full, without the written approval of EAG.**



Appendix

XRD Analysis Report  
EAG Number C0ENB225  
Sam McFadden  
Anamet, Inc.

Page 5 of 10  
24 Oct 2014

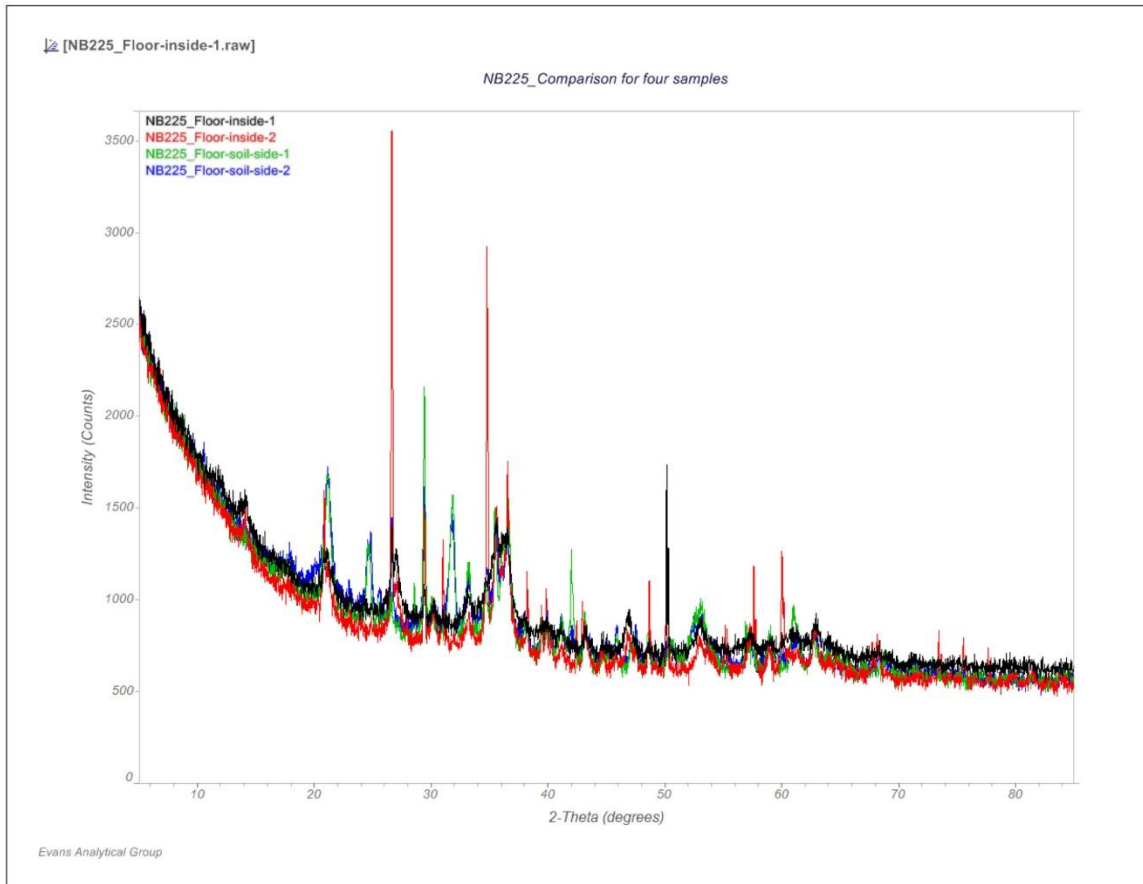


Figure 1: Comparison for four samples



Appendix

XRD Analysis Report  
EAG Number C0ENB225  
Sam McFadden  
Anamet, Inc.

Page 6 of 10  
24 Oct 2014

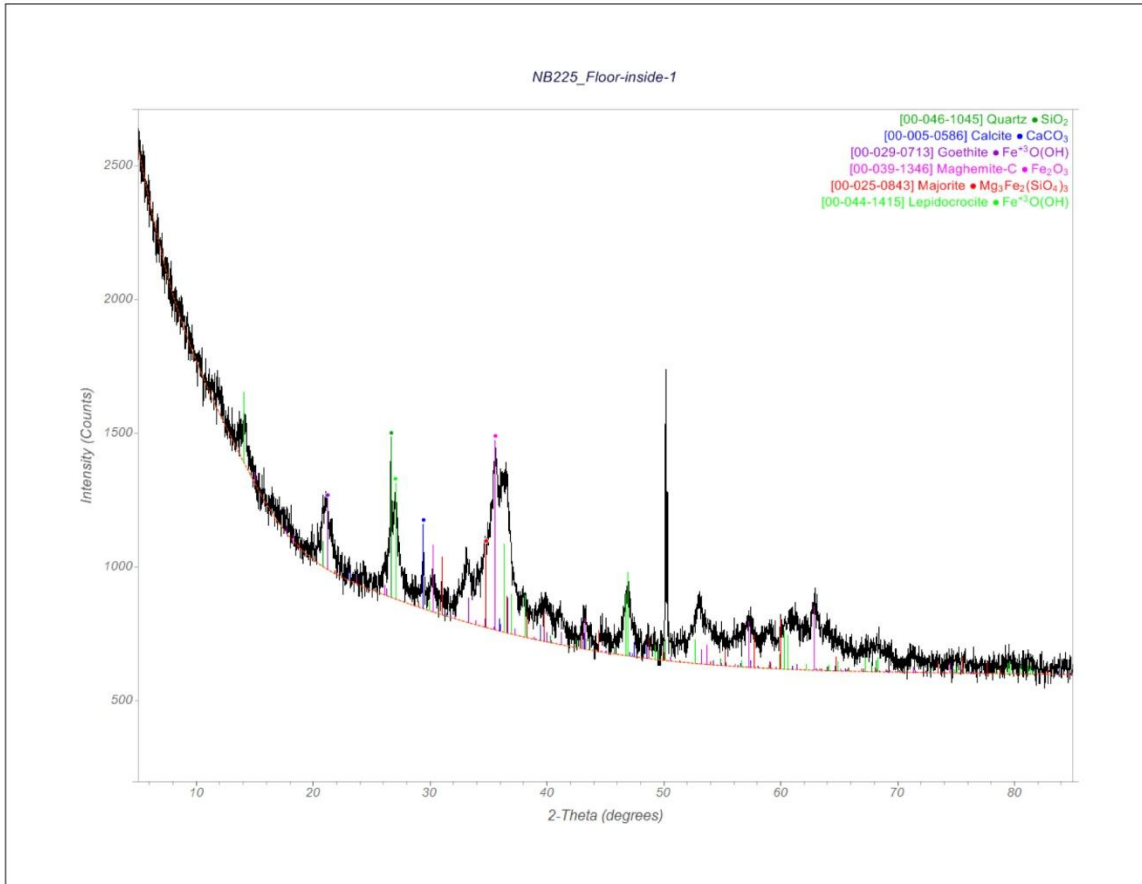


Figure 2: Phase identification for sample 1 (Floor inside surface #1)



Appendix

XRD Analysis Report  
EAG Number C0ENB225  
Sam McFadden  
Anamet, Inc.

Page 7 of 10  
24 Oct 2014

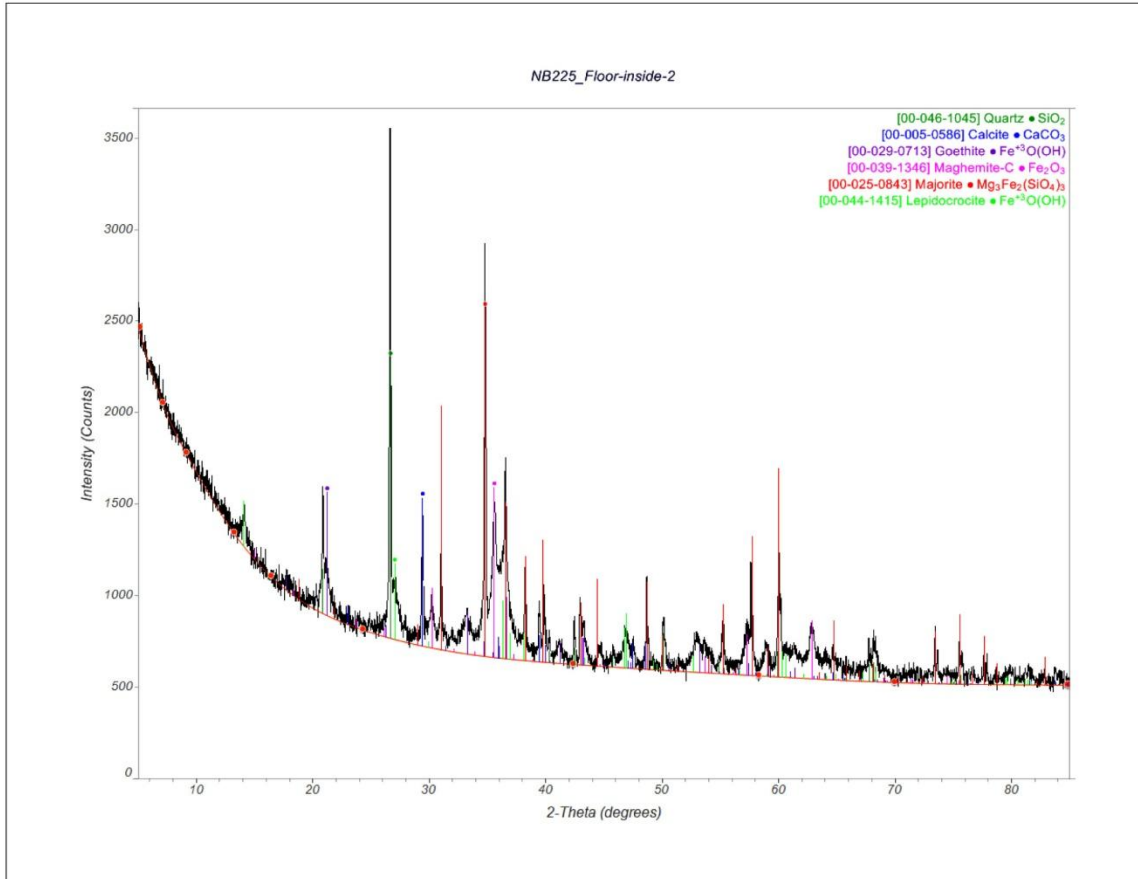


Figure 3: Phase identification for sample 2 (Floor inside surface #2)



Appendix

XRD Analysis Report  
EAG Number C0ENB225  
Sam McFadden  
Anamet, Inc.

Page 8 of 10  
24 Oct 2014

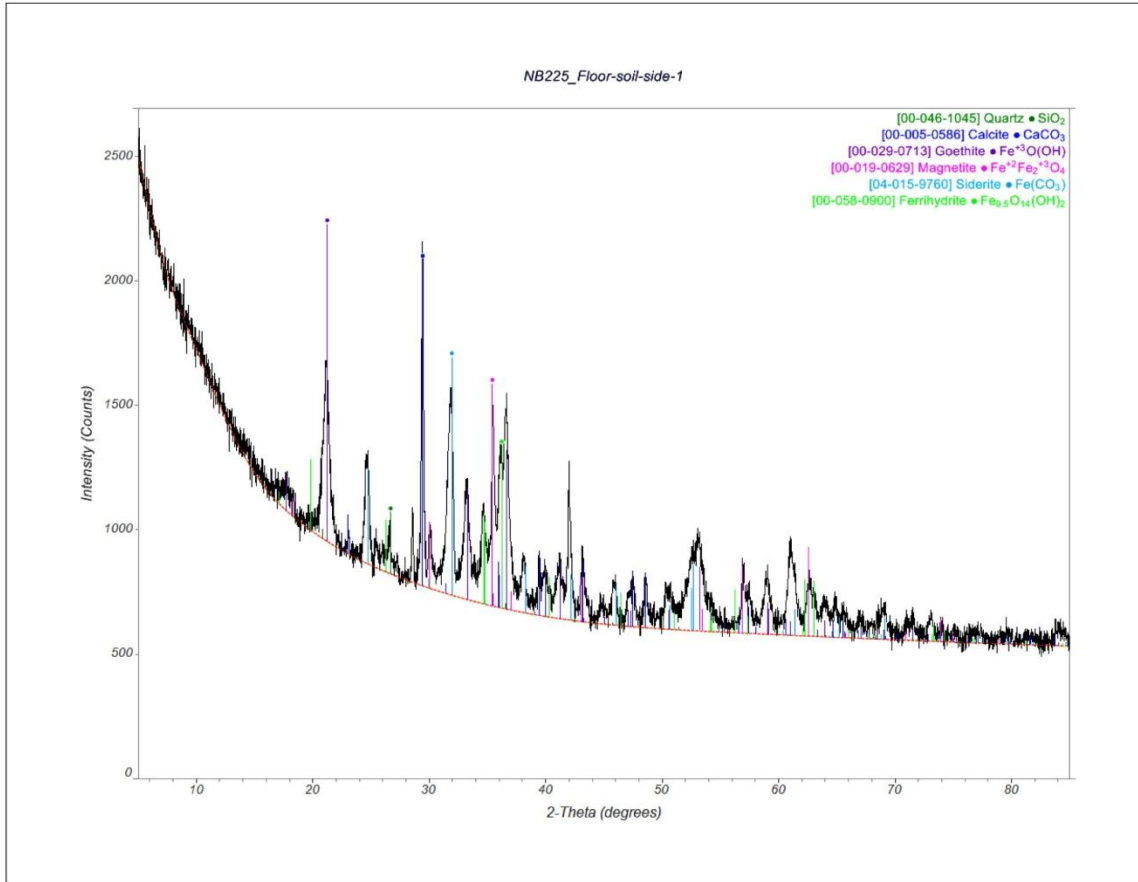


Figure 4: Phase identification for sample 3 (Floor soil side #1)

Appendix

XRD Analysis Report  
EAG Number C0ENB225  
Sam McFadden  
Anamet, Inc.

Page 9 of 10  
24 Oct 2014

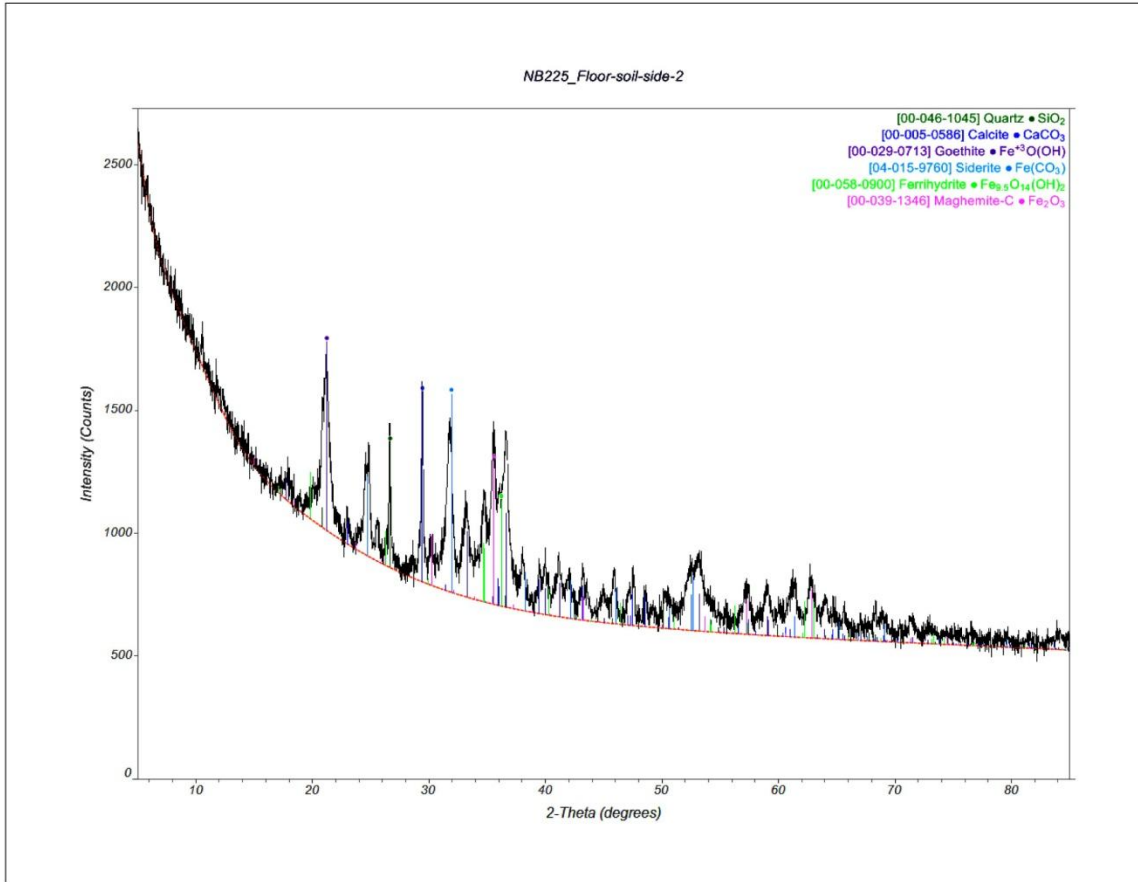


Figure 5: Phase identification for sample 4 (Floor soil side #2)



---

## Appendix

XRD Analysis Report  
EAG Number C0ENB225  
Sam McFadden  
Anamet, Inc.

Page 10 of 10  
24 Oct 2014

## Appendix

### Measurement Uncertainty:

There are two types of uncertainty in XRD analysis; uncertainty in the number of x-ray counts at a particular angle and uncertainty in the diffraction angle. Because the arrival of X-ray quanta in the detector is random with respect to time, the accuracy of X-ray counting rate measurements is governed by the laws of probability. In particular, the size of the one sigma standard deviation in an X-ray measurement is equal to the square root of the number of X-rays counted. A conservative criterion for the detection of a weak peak in a XRD pattern must have amplitude of greater than three standard deviations above background. As a result, the more slowly a measurement is made, the lower the relative standard deviation in the number of counts measured and the more likely is detection of trace diffraction peaks. If X-ray data is acquired at a constant speed, the relative standard deviation for the major diffraction peaks in a pattern will be on the order of a few percent or less while the relative standard deviation for the weaker peaks in a pattern will be on the order of tens of percent or more. This also implies that the uncertainty in the concentrations of the major phases in a sample will be lower than for the trace phases. Please note that there are a number of sample related factors that can influence peak intensity. These include (but are not limited to): average crystallite size, preferred orientation (texture), strain, and absorption.

Uncertainty in the position of X-ray diffraction peaks is due to both instrumental and sample effects. Instrumental position uncertainty is primarily due to diffractometer misalignment. Repeat measurements of NIST standard reference materials has shown that the maximum positional uncertainty is less than +/- 0.05 degrees 2-Theta and is typically much less than that. Positional uncertainty due to sample effects are related to sample displacement (displacement of the sample surface either above or below the diffractometer focusing circle) and sample transparency (the effect gets larger as the sample matrix becomes more transparent to the incident X-rays. Through careful sample preparation, the uncertainty due to these two sample effects should be less than +/- 0.03 degrees 2-Theta. Please note that in addition to these factors, solid solution effects, where one element is partially substituted for another within a given crystal structure, can produce significant shifts in measured peak positions. Unlike sample and instrumental peak position effects, solid solution effects can result in phase misidentification.